Monthly Notices of the ROYAL ASTRONOMICAL SOCIETY

MNRAS **499,** 5004–5021 (2020) doi:10.1093/mnras/staa3144
Advance Access publication 2020 October 27

K2-111: an old system with two planets in near-resonance

A. Mortier [1,2★] M. R. Zapatero Osorio,[3] L. Malavolta [4] Y. Alibert,[5] K. Rice [6,7] J. Lillo-Box,[3] A. Vanderburg,[8‡] M. Oshagh,[9,10] L. Buchhave [11] V. Adibekyan,[12,13,14] E. Delgado Mena,[12,13] M. Lopez-Morales,[15] D. Charbonneau,[15] S. G. Sousa [12,13] C. Lovis,[16] L. Affer,[17] C. Allende Prieto,[9,10] S. C. C. Barros,[12,13] S. Benatti,[17] A. S. Bonomo,[18] W. Boschin,[9,10,19] F. Bouchy,[16] A. Cabral,[20] A. Collier Cameron [21] R. Cosentino,[19] S. Cristiani,[22] O. D. S. Demangeon,[12,13,14] P. Di Marcantonio,[22] V. D'Odorico,[22,23] X. Dumusque,[16] D. Ehrenreich,[16] P. Figueira,[12,24] A. Fiorenzano,[19] A. Ghedina,[19] J. I. González Hernández,[9,10] J. Haldemann [5] A. Harutyunyan,[19] R. D. Haywood,[15,25‡] D. W. Latham,[15] B. Lavie,[16] G. Lo Curto,[26] J. Maldonado,[17] A. Manescau,[26] C. J. A. P. Martins [12,13] M. Mayor,[16] D. Mégevand,[16] A. Mehner,[24] G. Micela,[17] P. Molaro [22,23] E. Molinari,[27] N. J. Nunes,[20] F. A. Pepe,[16] E. Palle,[9,10] D. Phillips,[15] G. Piotto,[4] M. Pinamonti,[18] E. Poretti,[19,28] M. Riva,[28] R. Rebolo,[9,10] N. C. Santos,[12,13,14] D. Sasselov,[15] A. Sozzetti,[18] A. Suárez Mascareño,[9,10] S. Udry,[16] R. G. West [29] C. A. Watson[30] and T. G. Wilson [21†]

Affiliations are listed at the end of the paper

Accepted 2020 September 28. Received 2020 September 15; in original form 2020 July 29

ABSTRACT

This paper reports on the detailed characterization of the K2-111 planetary system with *K2*, WASP, and ASAS-SN photometry, as well as high-resolution spectroscopic data from HARPS-N and ESPRESSO. The host, K2-111, is confirmed to be a mildly evolved ($\log g = 4.17$), iron-poor ([Fe/H] = −0.46), but alpha-enhanced ([α/Fe]=0.27), chromospherically quiet, very old thick disc G2 star. A global fit, performed by using `PyORBIT`, shows that the transiting planet, K2-111 b, orbits with a period $P_b = 5.3518 \pm 0.0004$ d and has a planet radius of $1.82^{+0.11}_{-0.09}$ $R_\oplus$ and a mass of $5.29^{+0.76}_{-0.77}$ $M_\oplus$, resulting in a bulk density slightly lower than that of the Earth. The stellar chemical composition and the planet properties are consistent with K2-111 b being a terrestrial planet with an iron core mass fraction lower than the Earth. We announce the existence of a second signal in the radial velocity data that we attribute to a non-transiting planet, K2-111 c, with an orbital period of 15.6785 ± 0.0064 d, orbiting in near-3:1 mean motion resonance with the transiting planet, and a minimum planet mass of 11.3 ± 1.1 $M_\oplus$. Both planet signals are independently detected in the HARPS-N and ESPRESSO data when fitted separately. There are potentially more planets in this resonant system, but more well-sampled data are required to confirm their presence and physical parameters.

Key words: techniques: photometric – techniques: radial velocities – techniques: spectroscopic – planets and satellites: detection – stars: individual (K2-111).

1 INTRODUCTION

Planetary formation and evolution theories can improve only by discovering and characterizing a variety of planets around a variety of stars. An early example of this was the discovery of the first exoplanet around a solar-type star, 51 Peg b (Mayor & Queloz 1995), a hot Jupiter. This type of planet challenged planet formation theories that were at the time mainly based on the structure and composition of the Solar system.

Since then, space missions like *CoRoT*, *Kepler*, *K2*, and *TESS* (Borucki et al. 2010; Moutou et al. 2013; Howell et al. 2014; Ricker et al. 2015) have made extraordinary progress in exploring stars with a wide range of properties including spectral type, age, and location in the Galaxy, discovering thousands of planets and uncovering a wide variety of planetary systems. With radial velocity (RV) signatures of the smallest planets having semi-amplitudes of metres per second, or lower, high-resolution stable spectrographs, such as HARPS (Mayor et al. 2003) and HARPS-N (Cosentino et al. 2012), have been essential to further characterize these systems, precisely determining planetary masses and measuring the physical and chemical properties of the host stars. Newer generation spectrographs, like ESPRESSO (Pepe et al. 2014, 2020), will deliver long-term RV precision of 10 cm/s, a factor of at least 5 better than HARPS-N, and are thus expected to perform even better (as shown recently in Suárez Mascareño et al. 2020).

★ E-mail: angm2@cam.ac.uk
† Based on Guaranteed Time Observations collected at the European Southern Observatory under ESO programmes 1102.C-0744 and 1104.C-0350 by the ESPRESSO Consortium and at the Italian Telescopio Nazionale Galileo (TNG) by the HARPS-N Collaboration.
‡ NASA Sagan Fellow.

Next to precision, it is important to also ensure the accuracy of the measured parameters. In particular, for the planetary mass, having well-sampled RV data over a long time span has often been needed to cover a wide range of potential periods in the systems including the orbital periods of the known transiting planets, unknown orbital periods of additional planets, and the periods that may arise from stellar surface phenomena. Inadequate sampling or a few anomalous data points have been shown to make accurate mass measurements non-straightforward and even put planet detections in doubt (e.g. López-Morales et al. 2016; Rajpaul, Buchhave & Aigrain 2017; Cloutier et al. 2019).

Transiting planets offer the opportunity to characterize the planet's interior composition, since both the planetary mass and the radius, and thus its bulk density, can be determined. Having precisely determined elemental stellar abundances greatly helps in breaking the degeneracies between the models (e.g. Dorn et al. 2015, 2017; Hinkel & Unterborn 2018). Studies on the Solar system and exoplanetary systems show that the stellar and planetary composition are closely linked (e.g. Javoy et al. 2010; Santos et al. 2015, 2017; Thiabaud et al. 2015). Intense follow-up of small transiting exoplanets with high-resolution spectrographs provides many high-quality spectra allowing the precise determination of stellar elemental abundances, creating the unique opportunity to study the planet's internal structure.

K2-111, a slightly evolved G2 star, was found, with *K2* data, to have a transiting planet by Fridlund et al. (2017). They confirmed the existence of K2-111 b, a super-Earth ($R_p = 1.9 \pm 0.2\,R_\oplus$) with a period of 5.3512 d. From an extensive analysis of the stellar parameters, they found that the star, originally thought to be a Hyades member, was likely to be further away than the Hyades cluster and has an age of 10.8 ± 1.5 Gyr. It was clear from their work that a large investment of observing time to obtain RVs would be necessary to accurately and precisely characterize this system further. Less than 2 per cent of known exoplanets orbit a star older than 10 Gyr. With K2-111 thus being one of the oldest planet host stars ever discovered, this system covers a yet under-explored part of the stellar host parameter space.

The size of K2-111 b makes this system even more interesting as it lies on the right-hand side of the planet radius valley found for small exoplanets (e.g. Fulton et al. 2017; Zeng et al. 2017; Van Eylen et al. 2018). A precise planetary mass determination is thus crucial to understand whether this is a rocky planet or whether it has a large water layer or gas envelope.

The ESPRESSO and HARPS-N Science Teams have joined forces to obtain 154 precise RV observations of this system spanning over 4.5 yr. We describe in this paper how this effort resulted in a measured mass of the transiting planet K2-111 b, $M_p = 5.29\,M_\oplus$, with 7σ significance. This is $\sim$3 $M_\oplus$ lower than the value determined by Fridlund et al. (2017) but compatible within errors. We furthermore claim the presence of an additional non-transiting planet, K2-111 c, with a minimum mass of 11 $M_\oplus$ and a period of 15.678 d, making this planet orbit in near 3:1 resonance with the transiting planet K2-111 b. The long-time coverage of our RV data rules out the existence of the more massive outer companion, hypothesized by Fridlund et al. (2017).

The paper is structured as follows. Section 2 describes the obtained data, both from photometry and spectroscopy. We describe the star, including stellar activity in Section 3. A global fit of the data is described in Section 4. We then discuss the accuracy of the mass of K2-111 b, the origin of the additional strong signal in the data at 15.678 d, and potential additional signals in the data in Sections 5, 6, and 7, respectively. Finally, we discuss this system and conclude in Section 8.

2 OBSERVATIONS

2.1 *K2* photometry

K2-111 was observed as part of the fourth campaign of the *K2* mission (2015 February 7 to April 23).[1] It was observed in long cadence mode with integration times of 29.4 min totalling 3168 observations over 68.5 d.

We obtained the data from the Mikulski Archive for Space Telescopes (MAST[2]). The light curve was extracted following procedures described in Vanderburg & Johnson (2014), and the effects from the short time-scale spacecraft drift were corrected in a simultaneous fit of the transit shape, systematics, and low-frequency variations following Vanderburg et al. (2016).

Various extractions of a non-flattened *K2* light curve show no convincing evidence of rotation and allow us to rule out signals with amplitudes greater than about 2 ppt (parts-per-thousand) and periods less than about 70 d over the duration of the observation. In the remaining analyses, we used only the flattened light curve. The flattened and normalized light curves have flux uncertainties of 61 ppm (parts-per-million).

2.2 WASP photometry

K2-111 has been observed as part of the SuperWASP programme (Pollacco et al. 2006). The WASP photometric band roughly overlaps with the wavelength range of our spectroscopic data. In total, observations were taken over five seasons, ranging between 2004 July 29 and 2012 January 29 (i.e. spanning 7.5 yr). The seasons when data were taken are 2004–5, 2006–7, 2009–10, 2010–11, and 2011–12. The light curve was extracted following procedures described in Pollacco et al. (2006). Detrending for systematic effects was done by using SysRem (e.g. Collier Cameron et al. 2006; Mazeh, Tamuz & Zucker 2007). Stellar variability and potential transits are left in the data.

The resulting light curve was cleaned for outlier data points by performing a 5σ clip of the flux and removing points with unusually large errors. The final light curve, shown in Supplementary Fig. S1, contained 21118 data points over 236 nights and was scaled with the median of the light curve. The median error is 8 ppt, while the median error for the nightly binned data is 1 ppt. This light curve is thus not precise enough to detect the transiting planet, K2-111 b, which has a depth of 0.2 ppt, but it can be used to explore stellar variability (see Section 3.5).

2.3 ASAS-SN photometry

We obtained public *V*-band and *g*-band photometry via ASAS-SN[3] (Shappee et al. 2014; Kochanek et al. 2017). We have *V*-band observations over five consecutive seasons, from 2014 July till 2018 November, and *g*-band observations over three seasons, from 2017 September till 2020 March. The photometry thus overlaps roughly with our spectroscopic data.

We removed outlier data points with a 5σ clip on the flux. The final light curves, shown in Supplementary Fig. S1, contained 1152 data points over 337 epochs for the *g* band and 864 data points over 320 epochs for the *V* band. The median errors are 6 and 5 ppt for the *g* band and the *V* band, respectively. For nightly binned data, the

[1] Guest Observer Programmes: GO4060_LC, GO4033_LC, GO4007_LC.
[2] https://archive.stsci.edu/k2/
[3] Downloaded from https://asas-sn.osu.edu

Table 1. Example table of radial velocities and activity indicators for K2-111. The full table can be found in the online supplementary material.

Source	Time (BJD-2450000)	RV ($km\,s^{-1}$)	σ_{RV} ($km\,s^{-1}$)	FWHM ($km\,s^{-1}$)	σ_{FWHM} ($km\,s^{-1}$)	H α	$\sigma_{H\alpha}$	NaID	σ_{NaID}	S_{MW}	–
HARPS-N	7321.7177	−16.2835	0.0025	6.6726	0.0050	0.3177	0.0004	0.5475	0.0003	0.1637	–
HARPS-N	7323.5753	−16.2785	0.0024	6.6673	0.0049	0.3220	0.0005	0.5553	0.0003	0.1732	–
HARPS-N	7324.6572	−16.2826	0.0027	6.6753	0.0054	0.3150	0.0005	0.5604	0.0003	0.1768	–
ESPRESSO	8421.7397	−16.4084	0.0009	6.8739	0.0018	0.3048	0.0001	0.5347	0.0001	0.1688	–
ESPRESSO	8424.7793	−16.4061	0.0009	6.8763	0.0017	0.3055	0.0001	0.5314	0.0001	0.1700	–
ESPRESSO	8426.7576	−16.4012	0.0010	6.8765	0.0020	0.3042	0.0001	0.5313	0.0001	0.1663	–
–											

median errors get reduced to 3 ppt for both time series. These data are thus also not precise enough to detect the transits of small planets but can be used to study photometric variability (see Section 3.5).

2.4 HARPS-N spectroscopy

K2-111 was observed with the HARPS-N spectrograph (Cosentino et al. 2012), which is installed at the Telescopio Nazionale Galileo (TNG) in La Palma, Spain. HARPS-N has a resolving power $R \approx 115\,000$ and covers a wavelength range from 383 through 690 nm. The Guaranteed Time Observation (GTO) programme of the HARPS-N Collaboration obtained 104 observations. This was complemented with nine public observations (used in Fridlund et al. 2017).[4] The data were taken over three seasons, spanning 3.5 yr (2015 October 25 to 2019 February 24).

All 113 observations were taken with an exposure time of 1800 s and with the second fibre on the sky. The data were reduced using the standard Data Reduction Software (DRS – Baranne et al. 1996). A weighted cross-correlation function (CCF – Pepe et al. 2002) was obtained by using a G2 mask. All CCFs were subsequently corrected for the sky background and possible Moon contamination [see Malavolta et al. (2017a) for details]. RVs and the full width at half-maximum (FWHM) were obtained from a Gaussian fit of the corrected CCF. As the star is relatively faint, the errors are photon-limited, with a median RV error of 2.6 m/s. The RVs have an rms of 4.2 m/s, well above the median error.

From the 1D spectra, we also obtained the following measurements that could be an indicator of stellar activity (see e.g. Cincunegui, Díaz & Mauas 2007; Gomes da Silva et al. 2011, for details): H α, NaID, Mount Wilson S-index S_{MW}, and $\log R'_{HK}$ converted from the S-index following Noyes et al. (1984a). An example data table is in Table 1. In the online supplementary material, all data are provided in Table S2 and shown in Fig. S2.

To assess RV variations induced by stellar activity, we also computed chromatic RVs. These were computed by splitting the spectra in three different wavelength ranges (3830.0–4468.9 Å, 4432.6–5138.7 Å, and 5103.9–6900 Å).[5] The DRS provides the individual CCFs of each Echelle order, which we corrected for Moon contamination as mentioned above. We used the central wavelength of each order to establish if the corresponding CCF was within the specified wavelength range and then coadded all the CCFs within each wavelength range. We obtained the chromatic RVs via a Gaussian fit to the resulting CCFs. We estimated the RV error by taking into account the photon noise from the total counts of the coadded CCF and the read-out noise through the number of lines used in each order to build the CCF as returned by the DRS. We applied a correction factor to this estimate in order to closely reproduce the RV error from the full-spectrum CCF over a large range of SNR, knowing that the chromatic RVs will be inevitably noisier than the full-spectrum RVs.

2.5 ESPRESSO spectroscopy

We observed K2-111 with the fibre-fed Echelle Spectrograph for Rocky Exoplanets and Stable Spectroscopic Observations (ESPRESSO – Pepe et al. 2014, Pepe et al. 2020) installed at the incoherent combined Coudé facility of the Very Large Telescope (VLT) on the Paranal Observatory (Chile). A total of 41 ESPRESSO spectra were obtained as part of the GTO programmes 1102.C-0744, 1102.C-0958, and 1104.C-0350 between 2018 October 30 and 2020 March 3. There was a technical intervention on the instrument in the second half of 2019 June. This technical intervention led to a shift of the RV zero-point, and as a consequence, the two data sets have to be treated independently. We refer to the 16 and 25 spectra taken before and after this intervention as ESPRESSO 1 and ESPRESSO 2, respectively.

The typical exposure time per observation was 900 s and all data were taken with the HR21 mode (fibre size of 1 arcsec and 2 × 1 binning on the detector), the second fibre on the sky, and one of the VLT telescopes. The airmass of all observations was always lower than 2.2 to guarantee a good correction of the atmospheric dispersion.

ESPRESSO raw data were reduced with the DRS pipeline version 2.2.1, which included bias subtraction, correction for hot pixels, cosmic ray hits and flat-field, optimal extraction of the Echelle orders, sky subtraction, wavelength calibration using the combined Fabry-Perot – ThAr solution, and blaze correction. The ESPRESSO data have a mean resolving power $R \approx 138\,000$, cover wavelengths from 380 through 788 nm (going redder than HARPS-N), and have typical signal-to-noise (S/N) ratio of 45–80 at 550 nm (with few exceptions, which have lower S/N values).

We used the ESPRESSO sky-subtracted spectra to measure RVs. The pipeline provides a CCF for each ESPRESSO spectrum, which was built by using a G9 mask, an RV step of 0.5 $km\,s^{-1}$, and a systemic RV of -16.66 $km\,s^{-1}$. Similarly to HARPS-N data, ESPRESSO RVs and FWHMs were obtained from the Gaussian fit of the CCFs. We also obtained the same stellar-activity spectral indices from the sky-subtracted merged spectra as we did for the HARPS-N spectra. The final RVs have an rms of 3.7 m/s, well above the median RV error of 1.1 m/s. The ESPRESSO RV errors are like the HARPS-N RVs photon-noise-limited. An example data table is in

[4]Note that Fridlund et al. (2017) report 12 ARPS-N observations. However, three of those were taken with the second fibre in dark mode rather than the sky. We thus decided not to use these.

[5]This matches how the ESPRESSO chromatic RVs are derived with the exception of the lower blue and upper red boundary owing to HARPS-N's shorter wavelength range.

Table 2. K2-111 stellar properties.

Parameter	Value	Source
Designations and coordinates		
K2 ID	111	
EPIC ID	210894022	
2-MASS ID	J03593351+2117552	
Gaia DR2 ID	53006669599267328	
RA (J2000)	03:59:33.54	1
Dec (J2000)	+21:17:55.24	1
Magnitudes and astrometric solution		
B	11.80 ± 0.03	2
V	11.14 ± 0.04	2
G	10.9294 ± 0.0006	1
g	11.44 ± 0.04	2
r	10.95 ± 0.02	2
J	9.77 ± 0.02	3
H	9.48 ± 0.03	3
K	9.38 ± 0.02	3
W1	9.32 ± 0.02	4
W2	9.35 ± 0.02	4
W3	9.21 ± 0.03	4
Parallax π (mas)	4.9626 ± 0.0674	1
Distance d (pc)	201.7 ± 2.7	5
μ_α (mas/yr)	122.337 ± 0.182	1
μ_δ (mas/yr)	−35.438 ± 0.093	1
U (km/s)	−24.80 ± 0.90	5
V (km/s)	−103.96 ± 1.11	5
W (km/s)	60.48 ± 1.12	5

Note. 1: *Gaia* DR2 (Gaia Collaboration 2018); 2: UCAC-4 (Zacharias et al. 2012); 3: 2MASS (Cutri et al. 2003); 4: WISE (Cutri & et al. 2013); and 5: this work.

Table 1. In the online supplementary material, all data are provided in Table S2 and shown in Fig. S2.

Chromatic RVs (blue, green, and red) were also obtained with similar wavelength ranges as the HARPS-N chromatic RVs (except a longer range for the red RVs thanks to the extended wavelength range of ESPRESSO). Details on the extraction can be found in Suárez Mascareño et al. (2020).

The HARPS-N and ESPRESSO 1 RV time series overlap between 2018 October and 2019 February. This is convenient for defining a proper zero-point for the two data sets and finding a robust solution for the planetary system. The ESPRESSO RVs before and after the technical intervention on the spectrograph were treated as sets of data coming from two different instruments in our analysis.

3 STELLAR CHARACTERIZATION

In this section, we measure and refine all the parameters of the G2 star, K2-111, using new *Gaia* astrometry and our obtained photometric and spectroscopic data. All updated stellar property values are summarized in Tables 2 and 3.

3.1 Astrometry

Prior to the *Gaia* mission (Gaia Collaboration 2016), this star was thought to be part of the Hyades cluster of young stars (Pels, Oort & Pels-Kluyver 1975). However, with an improved new parallax and thus stellar distance, we now know that K2-111 (200.4 ± 2.7 pc – Bailer-Jones et al. 2018) is located behind the Hyades (47.50 ± 0.15 pc – Bailer-Jones et al. 2018) and is not part of it.

Table 3. K2-111 stellar properties.

Parameter	Value	Source
Atmospheric parameters		
$T_{\rm eff}$ (K)	5775 ± 60	1, 2
log g (cgs)	4.25 ± 0.15	1, 2
log g (cgs)	4.17 ± 0.01	1, 5
[Fe/H] (dex)	−0.46 ± 0.05	1, 2
ξ_t (km/s)	1.02 ± 0.05	1, 3
vsin i (km/s)	1.1 ± 0.5	1, 4
Elemental abundances		
[C/H] (dex)	−0.30 ± 0.06	1, 2
[O/H] (dex)	0.03 ± 0.07	1, 2
[Na/H] (dex)	−0.38 ± 0.02	1, 2
[Mg/H] (dex)	−0.14 ± 0.06	1, 2
[Al/H] (dex)	−0.22 ± 0.01	1, 2
[Si/H] (dex)	−0.27 ± 0.04	1, 2
[S/H] (dex)	−0.2 ± 0.07	1, 2
[Ca/H] (dex)	−0.24 ± 0.03	1, 2
[Sc/H] (dex)	−0.23 ± 0.09	1, 2
[Ti/H] (dex)	−0.16 ± 0.03	1, 2
[V/H] (dex)	−0.28 ± 0.04	1, 2
[Cr/H] (dex)	−0.43 ± 0.04	1, 2
[Mn/H] (dex)	−0.64 ± 0.05	1, 2
[Co/H] (dex)	−0.33 ± 0.03	1, 2
[Ni/H] (dex)	−0.41 ± 0.02	1, 2
[Cu/H] (dex)	−0.46 ± 0.07	1, 2
[Zn/H] (dex)	−0.26 ± 0.05	1, 2
[Sr/H] (dex)	−0.53 ± 0.08	1, 2
[Y/H] (dex)	−0.53 ± 0.06	1, 2
[Zr/H] (dex)	−0.42 ± 0.05	1, 2
[Ba/H] (dex)	−0.59 ± 0.06	1, 2
[Ce/H] (dex)	−0.60 ± 0.09	1, 2
[Nd/H] (dex)	−0.44 ± 0.04	1, 2
[α/Fe] (dex)	0.27	1, 5
Mass, radius, density, age		
M_* ($M_\odot$)	0.84 ± 0.02	1, 2, 6
R_* ($R_\odot$)	1.25 ± 0.02	1, 2, 6
ρ_* ($\rho_\odot$)	0.43 ± 0.02	1, 2, 6
ρ_* (g cm^{-3})	0.60 ± 0.03	1, 2, 6
Age t (Gyr)	$13.5^{+0.4}_{-0.9}$	1, 2, 6
Age t (Gyr)	12.3 ± 0.7	1, 2, 7

Note. 1: this work; 2: Adopted averaged parameters; 3: From ARES/MOOG analysis; 4: From SPC analysis; 5: using Mg, Si, Ti as the alpha abundance; 6: From isochrones analysis; and 7: From chemical clocks.

The *Gaia* DR2 RUWE (renormalized unit weight error) parameter, an indicator of the quality of the astrometric solution, is 1.22, which is towards the higher end (with RUWE peaking at 1.0 and RUWE >1.4 considered bad solutions). There is thus some evidence that the astrometric solution is noisy. Recent work has shown that this may indicate a hint of a more massive companion (Belokurov et al. 2020). Our RVs rule out a massive non-inclined companion, but a very inclined long-period massive companion could go undetected. *Gaia* DR3 will be required to shed more light on this.

Fridlund et al. (2017) derived Galactic space velocities and determined that the star is part of the thick disc population. We rederived these velocities using the *Gaia* DR2 data (Gaia Collaboration 2018). We used the RV value from *Gaia* Dr2 (RV = −16.66 ± 0.72 km/s) because *Gaia* has contrasted RV zero points. We also employed the trigonometric parallax and proper motions listed in Table 2 to calculate the U, V, and W heliocentric velocity components in the directions of the Galactic Centre, Galactic rotation, and

north Galactic pole, respectively, with the formulation developed by Johnson & Soderblom (1987). Note that the right-handed system is used and that we did not subtract the solar motion from our calculations. The uncertainties associated with each space velocity component were obtained from the observational quantities and their error bars after the prescription of Johnson & Soderblom (1987).

The large V and W components are a clear signpost that K2-111 kinematically belongs to the old population of the Galaxy, which agrees with the derived stellar age. More precisely, using the work from Reddy, Lambert & Allende Prieto (2006), and a Monte Carlo approach using 1 million samples, this star has a 97.41 ± 0.06 per cent probability of belonging to the thick disc, 2.35 ± 0.11 per cent probability of being a halo star, and 0.25 ± 0.06 per cent probability that it belongs to the thin disc. This high probability that K2-111 belongs to the thick disc agrees with the conclusion from Fridlund et al. (2017).

3.2 Stellar atmospheric parameters

We obtained stellar atmospheric parameters from the high-resolution HARPS-N spectra via three independent methods: ARES+MOOG,[6] `CCFPams`,[7] and SPC. Our final adopted parameters, listed in Table 3, are the average of the results from these three methods.

The ARES+MOOG method is explained in detail in Sousa (2014) and references therein. It is a curve-of-growth method based on neutral and ionized iron lines. Equivalent widths of these spectral lines were measured automatically from the stacked HARPS-N spectrum using `ARESv2` (Sousa et al. 2015). Effective temperature $T_{\rm eff}$, surface gravity $\log g$, iron abundance [Fe/H], and microturbulent velocity ξ_t are then determined by imposing excitation and ionization equilibrium. For this purpose, we used the radiative transfer code MOOG (Sneden 1973), assuming local thermodynamic equilibrium (LTE) and employing a grid of ATLAS plane-parallel model atmospheres (Kurucz 1993). Subsequently, the surface gravity was corrected for accuracy (Mortier et al. 2014) and we added systematic errors in quadrature to our precision errors for the effective temperature, surface gravity, and iron abundance (Sousa et al. 2011). We obtained $T_{\rm eff} = 5794 \pm 66$ K, $\log g = 4.35 \pm 0.11$, [Fe/H] $= -0.44 \pm 0.04$, and $\xi_t = 1.02 \pm 0.05$ km/s.

The `CCFpams` method uses the equivalent width of CCFs to obtain the effective temperature, surface gravity, and iron abundance via an empirical calibration. More detail on this method can be found in Malavolta et al. (2017b). Like the ARES+MOOG method, we subsequently corrected the surface gravity for accuracy. From this method, we obtained $T_{\rm eff} = 5762 \pm 34$ K, $\log g = 4.21 \pm 0.22$, and [Fe/H] $= -0.48 \pm 0.03$ (internal errors only).

Finally, the Stellar Parameter Classification tool (SPC) was used on the individual HARPS-N spectra. SPC is a spectrum synthesis method and is described in detail in Buchhave et al. (2012) and Buchhave et al. (2014). Final values were determined by the weighted average of the individual results, where the S/N ratio was used as the weight. Due to known issues related with the spectroscopic determination of the surface gravity (Torres et al. 2012; Mortier et al. 2014), we constrained this parameter by using isochrones. We obtained $T_{\rm eff} = 5769 \pm 49$ K, $\log g = 4.19 \pm 0.10$, and [m/H] $= -0.46 \pm 0.08$, and projected rotational velocity $v \sin i = 1.1 \pm 0.5$ km/s. SPC determines global metallicity assuming solar relative abundances for all the metals, while `CCFPams` and ARES+MOOG determine specifically iron abundance. Due to the overwhelming amount of iron lines in the HARPS-N wavelength range, these measures are treated as the same in this work.

We additionally analysed the stacked ESPRESSO spectrum with ARES+MOOG. The results were in full agreement with the results from the HARPS-N spectra: $T_{\rm eff} = 5779 \pm 62$ K, $\log g = 4.37 \pm 0.10$, [Fe/H] $= -0.47 \pm 0.04$, and $\xi_t = 1.06 \pm 0.03$ km/s. The two other methods (CCFPams and SPC) would require significant changes to the code and additional calibrated measurements in order to be applied to the ESPRESSO spectrum. We hence decided to adopt the averaged parameters from the HARPS-N spectra only.

The derived parameters show that K2-111 is mildly evolved, with a solar-like temperature but much more iron-poor than the Sun.

3.3 Stellar abundances

We used the stacked HARPS-N and stacked ESPRESSO spectra to derive elemental abundances for the following elements: C, O, S, Na, Mg, Al, Si, Ca, Ti, Cr, Ni, Co, Sc, Mn, V, Cu, Zn, Sr, Y, Zr, Ba, Ce, and Nd. We used the same setup as for the ARES+MOOG method described above and ran the analysis for these elements also in LTE, like we did for the atmospheric parameters. The methods are described in more detail in Adibekyan et al. (2012a), Mortier et al. (2013), Bertran de Lis et al. (2015), and Delgado Mena et al. (2017). All values are relative to the Sun, with the values of Asplund et al. (2009) as a reference for the solar values. In Table 3, we have averaged the individual values from the HARPS-N and ESPRESSO spectra.

We find that K2-111 is alpha-enhanced with [α/Fe] $= 0.27$ (using the average of the magnesium, silicon, and titanium abundances as the alpha-abundance). This is in line with the star belonging to the thick disc following (Adibekyan et al. 2012a). This is also confirmed by the enhanced [O/Fe] and [Zn/Fe]. The overall enhancement with respect to iron for these elements is in agreement with iron-poor planet hosts being generally enhanced more in alpha elements (Haywood 2009; Adibekyan et al. 2012b).

3.4 Stellar mass, radius, age, and distance

Stellar parameters were obtained from isochrones and evolutionary tracks. As input, we used the spectroscopically determined effective temperature and iron abundance, the *Gaia* DR2 parallax, and 11 magnitudes (listed in Table 2) ranging from the visible to the mid-infrared.

We used the code `isochrones` (Morton 2015), which uses `MultiNest` (Feroz et al. 2019) for its likelihood analysis. We ran the code three times, varying only between the three sets of spectroscopic parameters. We chose 400 live points, stellar models from the Dartmouth Stellar Evolution Database (Dotter et al. 2008), and constrained the prior on the age to be lower than log (Age/yr) $=$ 10.15. We extracted the final values and errors from the combined posteriors of these three runs, taking the median and the 16th and 84th percentile. These are the values reported in Table 3. The results of each individual run are all within 1σ of each other, owing to the agreement between the spectroscopic parameters.

We additionally tried obtaining parameters by using the models from the MESA isochrones and Stellar Tracks (MIST – Dotter 2016). However, the MultiNest evidences decisively favoured the Dartmouth models (with Bayes factors exceeding 10^9). Looking into this, we found that the MIST models as used by the `isochrones` package do not always interpolate well for stars older than 10 Gyr

[6] ARESv2: http://www.astro.up.pt/~sousasag/ares/; MOOG 2017: http://www.as.utexas.edu/~chris/moog.html
[7] https://github.com/LucaMalavolta/CCFpams

often giving back nan values. Since K2-111 is clearly older, it fails to find a good solution via the MIST models.

The stellar distance obtained via this method, 201.7 ± 2.7 pc, agrees very well with the one obtained by Bailer-Jones et al. (2018), 200.4 ± 2.7 pc. The surface gravity as calculated from the stellar radius and mass, $\log g = 4.17 \pm 0.01$, is much more precise than the spectroscopically determined surface gravity, but they do agree within 1σ. It confirms that the star is mildly evolved.

We found a stellar mass of $M_* = 0.84 \pm 0.02 M_\odot$ and a stellar radius of $R_* = 1.25 \pm 0.02 R_\odot$. Fridlund et al. (2017) determined the stellar mass and radius via three different methods. Our results agree within 1σ with two of their results (the DSEP and PARAM results). However, we do not find agreement with the stellar mass and radius they used to calculate their planetary mass and radius, which were higher ($1.0 \pm 0.07\,M_\odot$ and $1.4 \pm 0.14\,R_\odot$, respectively) than the values we obtained. This resulted in a systematic overestimation of the planetary mass and radius they reported as compared to ours.

From the isochrones analysis, we find that the age is $13.5^{+0.4}_{-0.9}$ Gyr. This is an older and more precise stellar age than the one reported by Fridlund et al. (2017), who reported 10.8 ± 1.5 Gyr. Stellar evolution models are, however, not designed for stars this old. We additionally made use of the stellar chemical abundances to calculate ages by using the so-called chemical clocks (i.e. certain chemical abundance ratios that have a strong correlation for age). We applied the 3D formulas described in table 10 of Delgado Mena et al. (2019), which also consider the variation in age produced by the effective temperature and iron abundance [Fe/H]. The chemical clocks [Y/Mg], [Y/Zn], [Y/Ti], [Sr/Ti], and [Sr/Zn] were used from which we took a weighted average. We derive an age of 12.3 ± 0.7 Gyr. This is lower than the isochrone-constrained age but still points to a very old star. From the study of Nissen et al. (2020), it is also clear that the chemical composition of K2-111 is consistent with the star being very old. While we thus may not accurately determine the age of this system, we do show that it is very likely older than 10 Gyr. This agrees with the kinematic behaviour of this star pointing to a thick disc.

3.5 Stellar activity

Signals arising from stellar activity are the main barrier in detecting small exoplanets in RVs and accurately and precisely measuring their mass (e.g. Haywood et al. 2014; Rajpaul et al. 2015; Mortier et al. 2016; Dumusque et al. 2017). It is thus paramount to understand the star, its rotation period, and the strength of possible activity effects to the best of our ability. We have used both photometric and spectroscopic data for this purpose.

3.5.1 From photometry

The WASP data were taken years before the first RVs were observed. However, given its 7.5-yr data span, it could give us insight into the stellar rotation period and the overall photometric variability. The rms of the full light curve is equal to the median error, 8ppt. Split into the five seasons, we find that the third season was marginally the most quiet with an rms of 6ppt while the first season had the largest rms of 10 ppt. Using the nightly binned data reduced the rms to 1–2 ppt, again equal to the median error. Any stellar variability during the time span of the data is thus likely lower than or at the level of the data errors.

We applied a Bayesian General Lomb–Scargle periodogram (BGLS – Mortier et al. 2015) to the full WASP light curve and to the five seasons separately. This is shown in Fig. 1. Using all data or nightly binned data does not affect the shape of the periodograms. For most seasons, no strongly significant periodic signals are evident, with the exception of season 2 (2006–2007). This season contains the most data points and shows its strongest peaks at 27.5, 14, and 52 d. These could be related to the rotation of the star. We caution, however, that the strength of the 27.5-d periodicity may be partly sampling-related due to avoiding Moon-lit nights. Indeed, when we phase-fold the data in season 2 with a period of 27.5 d, an obvious phase gap is present coinciding with a full Moon.

The BGLS periodogram of the full data shows forests of peaks at 28, 14, and 50 d, all coinciding with the BGLS periodogram from season 2. Additionally, the BGLS periodogram of the full data shows periodicity around 5.8 d. Given the age, evolutionary status, and projected rotational velocity of K2-111 (see Section 3), it is highly unlikely that this is related to the rotation period. However, it is important to bear in mind that this photometric variability is present, given its period is close to the orbital period of the transiting planet, K2-111 b.

As a second investigation, we applied a Gaussian Process (GP) regression with a quasi-periodic kernel to the full WASP data. We used the nightly binned data, normalized with the median of the data, since that speeds up the process considerably and the periodograms of binned and unbinned data look similar. We used a quasi-periodic covariance kernel (as described in e.g. Grunblatt, Howard & Haywood 2015; Dubber et al. 2019) and allowed for additional white noise. The `PyORBIT` code (Malavolta 2016) was used to do the analysis and `MultiNest` was used for the parameter inference, with 400 live points. We constrained the rotation period to be lower than 100 d, the decay time-scale to be lower than 1000 d, and the coherence scale to be between 0.2 and 2.0, shown by several works (e.g. Haywood et al. 2014; Dubber et al. 2019) to be the most physically motivated for stellar activity phenomena.[8] Taking the median, 16th and 84th percentile of the posterior distributions, the results are as follows: rotation period $P_{\rm rot} = 27.4^{+1.4}_{-1.2}$ d, decay time-scale $P_{\rm dec} = 83^{+255}_{-51}$ d, amplitude $h = 1.2 \pm 0.3$ ppt, coherence scale $w = 0.32^{+0.32}_{-0.09}$, and white noise $s = 1.2 \pm 0.2$ ppt. This model is clearly preferred over a white-noise-only model with a Bayes factor[9] exceeding 10^5.

We repeated the same process for the ASAS-SN data. The rms of the full light curve is 13 and 8 ppt for *g* band and *V* band, respectively. A higher rms for blue with respect to red wavelengths is expected if the star is faculae-dominated instead of spot-dominated. Using the binned data reduces the rms to 10 and 6 ppt, respectively. Both these values are higher than the median error and higher than the results from the WASP light curve. Since the WASP and ASAS-SN data are not concurrent, with at least 2 yr between the end of the WASP data and the start of the ASAS-SN data, this could suggest that K2-111 was in a quieter part of its activity cycle when the WASP data were taken and slightly more active at the time of the RV observations or it could be a simple consequence of the WASP data being more precise. In any case, overall these rms values are still fairly low. Using the binned data, we find that the *V*-band data are reasonably constant in rms. The rms of the seasonal *g*-band data increases with each season. It is noteworthy that this is in contrast with the average *S* index going down over the same seasons as shown in the next Section.

[8]Not constraining the coherence scale led to multimodal posterior distributions and a coherence scale of 0.08.

[9]We use the Nested Importance Sampling global evidences to compute Bayes factors throughout this work (Feroz et al. 2019).

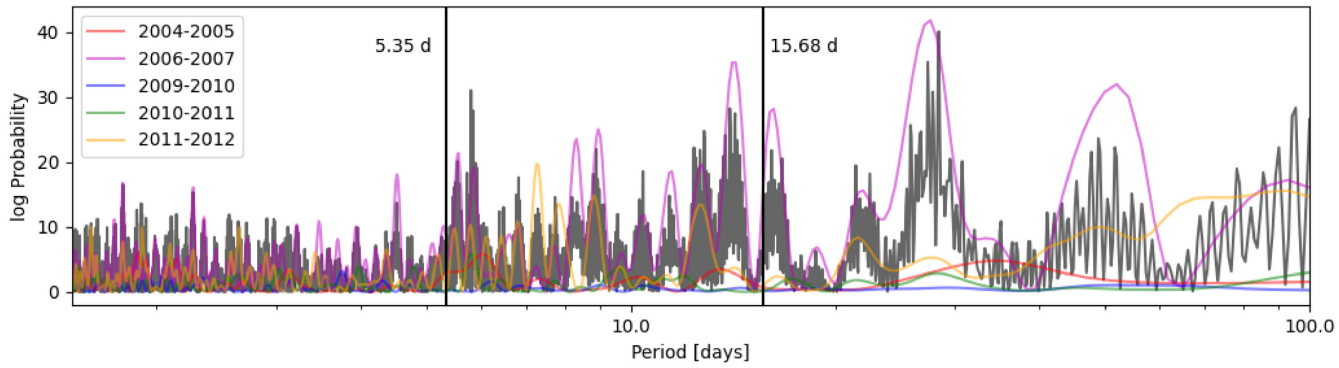

Figure 1. BGLS periodogram for the full WASP data (black curve) and the individual seasons (coloured curves). The two vertical lines indicate the periods of the transiting planet and the strongest RV signal at 15.678 d.

The BGLS periodogram of the ASAS-SN data is shown in Fig. 2. As expected from the rms values, the *g*-band data show stronger periodicities than the *V*-band data with the latter not showing any significant periodicities. For the *g*-band data, the first season shows the strongest periodicities at 14.9, 28, and 9 d, similar to the WASP data. We do still have to caution that this variability may be partly related to the cycle of the Moon. When the first season of data is phased up with the Moon phases, the quadratures do appear to be close to full and new Moon. The second season also identifies some periodicity at 5.5 d, slightly higher than the period of K2-111 b.

For the ASAS-SN binned data, we also ran a GP regression in a similar fashion as described above. For both data sets, the model with GP was decisively preferred over a model with white noise only. The results are as follows for the *g*-band data: $P_{\rm rot} = 28.1^{+1.2}_{-0.2}$ d, $P_{\rm dec} = 571^{+312}_{-387}$ d, $h = 11.9^{+8.6}_{-4.6}$ ppt, $w = 0.94^{+0.55}_{-0.32}$, and white noise $s = 8.0 \pm 0.4$ ppt. The value for the rotation period broadly agrees with the results from the WASP data but all other parameters are larger. The large amplitude is worrisome, given that the *K2* photometry firmly ruled these amplitudes out. The *g*-band is bluer than the Kepler band, so stellar signals could be expected to be somewhat larger there, but it could also be that this is a spurious signal, not related to the rotation of the star. The *V*-band data gave $P_{\rm rot} = 31.2^{+5.8}_{-7.9}$ d, $P_{\rm dec} = 105^{+70}_{-51}$ d, $h = 2.9^{+0.8}_{-0.6}$ ppt, $w = 0.83^{+0.69}_{-0.38}$, and white noise $s = 4.3 \pm 0.4$ ppt, in better agreement overall with the WASP data, but still larger than what we would expect given the *K2* data.

In total, all our photometry spans almost 15 yr. A GP regression was thus also run on all three photometry data series simultaneously. The rotation period, decay time-scale, and coherence scale were kept the same across all three data series as these values are inherent to the star. The amplitude and white noise could vary per data set. Since each data set was taken in a different photometric band, we would not expect the amplitude to be the same across the data sets. The results are $P_{\rm rot} = 29.2 \pm 0.8$ d, $P_{\rm dec} = 74^{+48}_{-23}$ d, and $w = 0.59^{+0.17}_{-0.12}$. The amplitudes for the WASP, ASAS-SN *g*-band, and ASAS-SN *V*-band data, respectively, are 1.2 ± 0.3, $6.0^{+1.5}_{-1.0}$, and 2.8 ± 0.6 ppt, with additional white noise of $s = 1.3 \pm 0.1$, 7.8 ± 0.4, and 4.2 ± 0.3 ppt.

From the sheer length of the complete data set, it seems plausible from the WASP and ASAS-SN photometry that the stellar rotation period of K2-111 is indeed around 29 d but with relatively low amplitude. However, the *K2* photometry, even though shorter in time span, does not corroborate such a signal. We injected signals with a period of 27 d into the *K2* light curve with varying amplitudes. Based on a visual inspection of the results, we expect that if such a signal was present in the *K2* light curve with a semi-amplitude greater than about 500 ppm, we likely would have detected it. There is thus still a chance that the variations seen in the other photometry are influenced by Moon light and thus exaggerated. We estimated the expected RV rms based on the photometry variations we see using the results of Hojjatpanah et al. (2020), which are based on *TESS* photometry. While there is large scatter in their relations and considering the *TESS* passband is redder than the photometry used here, we cannot exclude 1–2 m/s rms due to stellar activity in our data.

3.5.2 *From spectral indicators*

Next, we investigated any effects from stellar activity seen in the spectra and its derivative measurements. For this we used the measured projected rotational velocity and five different activity indicators, namely FWHM, Hα, NaID, $S_{\rm MW}$, and $\log R'_{\rm HK}$.

A rough constraint on the rotational period can be set by using the projected rotational velocity and the stellar radius and assuming a stellar inclination of 90 degrees. Using the values in Table 3, we get $P_{\rm rot} = 57^{+48}_{-18}$ d from drawing 10 000 samples. Due to degeneracies between the various broadening mechanisms, given our spectral resolution, it is possible to define only an upper limit of 2 km/s for stars rotating slower than that. If we thus use the latter value as an upper boundary, we find that the rotational period should be higher than 31.6 ± 0.5 d. While both these values are higher than the 29-d period derived from the photometry, it is worth bearing in mind that the stellar inclination is likely not exactly 90 degrees and the actual rotation periods are thus likely a bit lower. A rotation period of 29 d is thus not excluded from the projected rotational velocity and stellar radius.

We also investigated the stellar activity indicators derived from the spectra. For this investigation, we subtracted three offsets from the RVs for the HARPS-N, ESPRESSO 1, and ESPRESSO 2 data, respectively. These offsets were derived from the final global fits: −16.27535, −16.40504, and −16.40844 km/s, respectively. We also subtracted the median value of FWHM for each of these three data sets since the FWHM of the CCF is instrument- and pipeline-dependent. The other indicators should be independent from the instrument, so no values were subtracted for those indicators. We note that due to some interstellar clouds between us and K2-111, and the corresponding extra Na absorption lines [shown in Fridlund et al. (2017) and confirmed in our spectra], the NaID index may be contaminated.

Fig. 3 shows the BGLS periodogram for the RVs as well as the indicators. The BGLS periodogram for $\log R'_{\rm HK}$ has the same

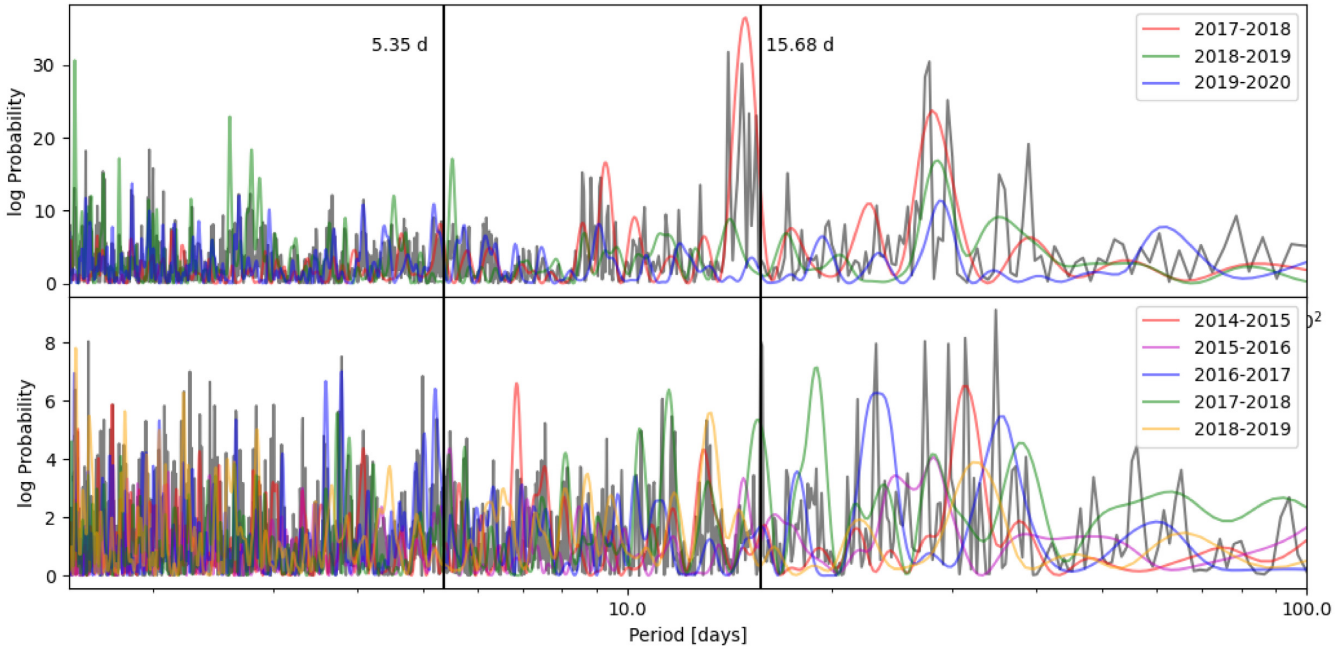

Figure 2. BGLS periodograms for the full ASAS-SN data (black curve) and the individual seasons (coloured curves). Top plot is for *g*-band data and bottom plot for *V*-band data. The two vertical lines indicate the periods of the transiting planet and the strongest RV signal at 15.678 d.

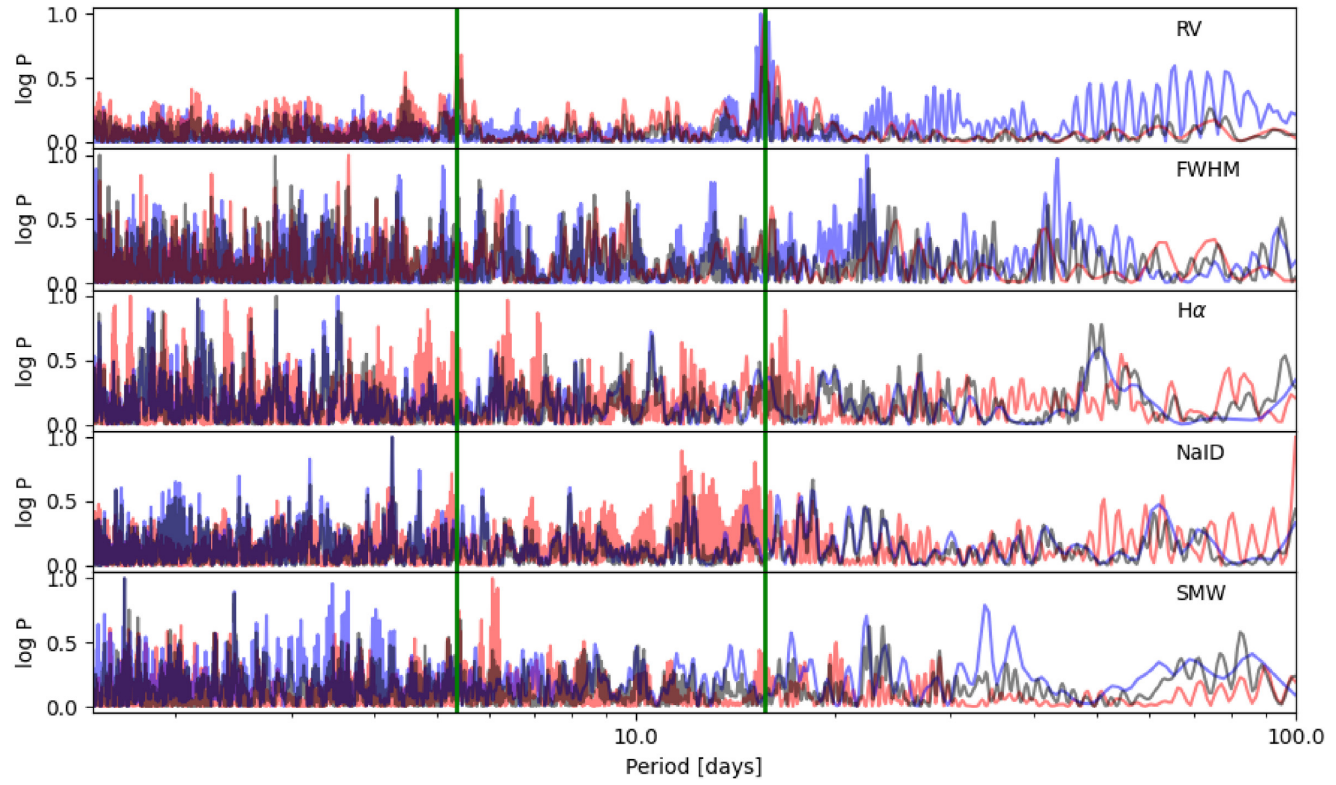

Figure 3. BGLS periodograms for, from top to bottom, RV, FWHM, H α, NaID, and S-index. The blue curve is for HARPS-N data, the red curve for ESPRESSO data, and the black curve for the combined data with the appropriate offsets applied where necessary. The green vertical lines indicate the transiting planet period, 5.35 d, and the strongest periodicity seen in the RVs, 15.68 d. The *y*-axis, showing the period posterior probability, has been normalized to be between 0 and 1.

shape as the S-index and is not shown. The periodograms have been normalized to put the maximum at 1. The periodograms of the RVs for both instruments show its highest peak at 15.678 d. The ESPRESSO RVs show additional peaks at the period of K2-111 b, 5.35 d, and also at 4.47 d. The HARPS-N RVs show marginal power at 5.35 d but some more peaks at higher periods, with forests of peaks around 23 d, 30 d, and higher than 50 d.

In contrast with the RV periodogram, the periodograms of the indicators are not as clear and no strong periodicities stand out. Crucially, none of the indicators show any power around 29 d, casting doubt on the origin of the 29 -d signal in the photometry. The HARPS-N FWHM displays periodicities around 43, 22, and 13 d, suggesting that the rotation period could perhaps be as high as 43 d where the other periodicities would be the harmonics. None of these periodicities are strong enough to draw a firm conclusion and they are not replicated in the other indicators either. The S-index shows different behaviour for each instrument, with marginally likely periodicities at 6 d for ESPRESSO and 34 d for HARPS-N. Overall, the periodicities in the activity indicators (or lack thereof) suggest that K2-111 is a quiet star. This is not unexpected given its old age.

The S-index and associated log $R'_{\rm HK}$ are traditionally seen as an excellent indicator for a star's magnetic cycle. The Sun, for example, has an S-index varying between 0.16 and 0.18 throughout its 11-yr magnetic cycle (e.g. Egeland et al. 2017). There is a hint that the S-index of K2-111 goes down over the course of the RV observations, with a median S-index going from 0.171 in the first season of data to 0.165 in the final season of data. The median log $R'_{\rm HK}$ goes from -4.91 to -4.94 with an overall median value of -4.93. Using the calibrations from Noyes, Weiss & Vaughan (1984b) and Mamajek & Hillenbrand (2008), this median value of log $R'_{\rm HK}$ would indicate a rotation period of 25 d, but these calibrations are not well tested for stars as old or alpha-enhanced as K2-111.

The average value of log $R'_{\rm HK}$ can be used to estimate the expected stellar-induced RV variations. From equation (1) of Hojjatpanah et al. (2020), a value of -4.93 for log $R'_{\rm HK}$ translates to an RV rms of 2.85 m/s. Many stars included in their fit were, however, rotating much faster than K2-111. In contrast, Suárez Mascareño et al. (2017) estimates that the RV semi-amplitude induced by stellar activity variations of a G dwarf with average log $R'_{\rm HK}$ of -4.9 should be lower than 1 m/s, though this was based on a smaller sample. Recent HARPS-N solar data show an rms of 1.63 m/s (Collier Cameron et al. 2019) while the Sun was approaching Solar minimum with values of log $R'_{\rm HK}$ around -4.97. We can thus reasonably expect RV variations from stellar activity at the level of 0.5–3 m/s.

Due to the lack of common periodicities between the RVs and the spectral indicators, it is no surprise that there is little to no correlation between these values. Pearson and Spearman correlation coefficients of the RVs and indicators are all between -0.2 and 0.2, indicating no significant correlation between RVs and the indicators.

To conclude, K2-111 appears to be a chromospherically quiet star. The rotation period cannot be uniquely determined from the plethora of data and indicators. The photometry points marginally to a rotation period of 29 d, while the spectroscopic indicators point marginally to 25 or 43 d and do not confirm clear variability at 29 d. The RVs show no sign of strong periodicities at any of these periods.

4 GLOBAL FIT

We performed a global fit to the data (the *K2* photometry and HARPS-N and ESPRESSO RVs) using the `PyORBIT` code (Malavolta et al. 2016). We used `MultiNest` for the parameter inference with 1000 live points. The photometric transit was modelled using the `batman` transit model (Kreidberg 2015), quadratic limb darkening, and an exposure time of 1764.944 s for the photometry to account for the long-cadence observations following Malavolta et al. (2018). Eccentricity e and longitude of periastron ω were combined in the fitting parameters $\sqrt{e}\cos\omega$ and $\sqrt{e}\sin\omega$ as per the recommendations of Eastman, Gaudi & Agol (2013). All priors were either uniform or log-uniform (the latter in the case of the semi-amplitudes for all Keplerians and the periods of the non-transiting Keplerian signals) and are listed in Table 4. White noise, additional to the errors, and an offset was included per instrument, where the ESPRESSO 1 and ESPRESSO 2 data were considered to be from two different instruments.

Given the strong periodicity of 15.68 d seen in the RV BGLS periodogram, we ran a model including two Keplerians, one relating to the transiting planet K2-111 b, and one relating to this periodicity of 15.678 d (the period was constrained to be between 10 and 20 d

Table 4. K2-111 system parameters from combined fit.

Parameter	Prior	Value
Stellar parameters		
ρ_* ($\rho_\odot$)	$\mathcal{N}(0.43, 0.02)$	
LD coefficient q_1	$\mathcal{U}(0, 1)$	0.55 ± 0.28
LD coefficient q_2	$\mathcal{U}(0, 1)$	$0.42^{+0.33}_{-0.28}$
Systemic velocities:		
γ_{HN} (m/s)	$\mathcal{U}(-16280, -16270)$	-16275.2 ± 0.3
γ_{E1} (m/s)	$\mathcal{U}(-16450, -16350)$	-16405.3 ± 0.6
γ_{E2} (m/s)	$\mathcal{U}(-16450, -16350)$	-16408.5 ± 0.4
White noise:		
$s_{\rm j,\,HN}$ (m/s)	$\mathcal{U}(0.01, 10)$	$1.50^{+0.42}_{-0.46}$
$s_{\rm j,\,E1}$ (m/s)	$\mathcal{U}(0.01, 10)$	$1.75^{+0.77}_{-0.67}$
$s_{\rm j,\,E2}$ (m/s)	$\mathcal{U}(0.01, 10)$	$1.39^{+0.38}_{-0.32}$
$s_{\rm j,\,K2}$ (ppm)	$\mathcal{U}(1, 6100)$	7^{+5}_{-4}
Transit and orbital parameters		
$P_{\rm b}$ (d)	$\mathcal{U}(5.34, 5.36)$	5.3518 ± 0.0004
$T_{\rm tr,b}$ (BJD-2450000)	$\mathcal{U}(7100.0, 7100.2)$	$7100.0768^{+0.0019}_{-0.0018}$
T_{14} (d)		$0.133^{+0.015}_{-0.020}$
$R_{\rm p,\,b}/R_*$	$\mathcal{U}(0.00001, 0.5)$	$0.01346^{+0.00074}_{-0.00061}$
$i_{\rm b}$ (deg)		$86.43^{+0.37}_{-0.21}$
Impact parameter $b_{\rm b}$	$\mathcal{U}(0, 1)$	$0.66^{+0.11}_{-0.12}$
$\sqrt{e_{\rm b}}\cos\omega_{\rm b}$	$\mathcal{U}(-1, 1)$	$0.11^{+0.15}_{-0.14}$
$\sqrt{e_{\rm b}}\sin\omega_{\rm b}$	$\mathcal{U}(-1, 1)$	$-0.25^{+0.33}_{-0.23}$
$e_{\rm b}$		$0.13^{+0.13}_{-0.09}$
$\omega_{\rm b}$ (rad)		$-1.21^{+1.29}_{-0.48}$
$K_{\rm b}$ (m/s)	$\mathcal{LU}(0.01, 100)$	2.21 ± 0.32
$P_{\rm c}$ (d)	$\mathcal{LU}(10, 20)$	$15.6785^{+0.0064}_{-0.0063}$
Phase $\phi_{\rm c}$ (rad)	$\mathcal{U}(0, 2\pi)$	1.38 ± 0.20
$\sqrt{e_{\rm c}}\cos\omega_{\rm c}$	$\mathcal{U}(-1, 1)$	$0.05^{+0.21}_{-0.22}$
$\sqrt{e_{\rm c}}\sin\omega_{\rm c}$	$\mathcal{U}(-1, 1)$	0.00 ± 0.20
$e_{\rm c}$		$0.07^{+0.07}_{-0.05}$
$\omega_{\rm c}$ (rad)		$-1.39^{+1.68}_{-2.62}$
$K_{\rm c}$ (m/s)	$\mathcal{LU}(0.01, 100)$	$3.27^{+0.31}_{-0.32}$
Planetary parameters		
$M_{\rm p,b}$ ($M_\oplus$)		$5.29^{+0.76}_{-0.77}$
$R_{\rm p,b}$ ($R_\oplus$)		$1.82^{+0.11}_{-0.09}$
$\rho_{\rm p,\,b}$ (g cm^{-3})		4.8 ± 1.0
$a_{\rm b}$ (AU)		0.0570 ± 0.0012
$M_{\rm p,c}\sin i$ ($M_\oplus$)		11.3 ± 1.1
$a_{\rm c}$ (AU)		0.1166 ± 0.0025

Note. For the priors, $\mathcal{N}$ indicates a Gaussian prior with mean and standard deviation. $\mathcal{U}$ indicates a uniform prior, and $\mathcal{LU}$ a log-uniform prior with logarithm base 2 where the values within parentheses indicate the minimum and maximum values.

to speed up the `MultiNest` run). We allowed both orbits to be eccentric. The resulting orbits are shown in Fig. 4, the parameters listed in Table 4, and the corner plots of the fit parameters shown in Figs S3 and S4 in the online supplementary material.

The fit converges to two low-eccentricity orbits, with the transiting planet ($P = 5.3518$ d) fitted with a slightly higher eccentricity ($e = 0.13$) than the second signal at 15.678 d ($e = 0.07$). Both eccentricities are, however, consistent with zero at the 2σ level. The transiting planet K2-111 b has its radius ($1.82\,R_\oplus$) determined with 20σ significance. The mass of K2-111 b is fitted as $5.29\,M_\oplus$, significant to almost 7σ.

The best-fitting white noise was between 1.4 and 1.8 m/s depending on the instrument, with the first season of ESPRESSO having the largest white noise. This value is consistent with the estimates derived in Section 3.5. We ran the same model multiple times to check whether the nested sampling algorithm found consistent results, which was the case. The residual rms of the HARPS-N and ESPRESSO data, respectively, is 3.3 and 2.1 m/s. This is in agreement with the expected rms, given the RV errors and fitted white noise.

A fit with only the transiting planet was run in order to assess the model evidences. A 2-Keplerian model was very strongly favoured with Bayes factors exceeding 10^{10}. Similarly, a model was run where the two Keplerians were kept circular. This circular model was preferred but only with a Bayes factor of 51, which is not decisive [Kass & Raftery (1995) recommend a Bayes factor higher than 150]. Since there is no physical reason to prefer circular orbits over moderately eccentric ones for K2-111, we chose to stick with the eccentric solutions, even though both fitted eccentricities are fully consistent with zero.

In the next sections, we discuss the mass accuracy of K2-111 b, as well as the origin of the strong sinusoidal signal at 15.678 d. The residuals of this 2-Keplerian model also show some periodicity between 60 and 65 d and lots of forested peaks of periodicity at periods lower than 10 d, as shown from the BGLS periodogram in Fig. 5. We discuss this further in Section 7.

5 ACCURACY OF THE MASS OF K2-111 B

The mass of the transiting planet K2-111 b is precisely determined, with 1σ errors one-seventh of the median value. However, it is important to also assess the accuracy of the fitted mass. Inadequate sampling and/or models can influence the accuracy of the extracted parameters and, in particular, the semi-amplitudes and thus planetary masses. An extreme example of this is Kepler-10 c, where HIRES and HARPS-N data found very discrepant mass estimates (Dumusque et al. 2014; Weiss et al. 2016). Investigating this, Rajpaul et al. (2017) showed that the discrepancy could possibly be explained by sub-optimal sampling and/or the model choice.

We analysed the HARPS-N and ESPRESSO data separately to assess the mass accuracy of K2-111 b. The larger number of data points from HARPS-N could be balanced against the higher precision of the ESPRESSO data making both data sets qualitatively comparable. It is thus reasonable to expect comparable results by analysing the data sets separately. We ran a global fit (including the *K2* photometry) assuming a 2-Keplerian eccentric model on the separate data sets. Similar priors, boundaries, and live points were used as for the full global fit. Using the HARPS-N data, we found a planet mass $M_{\rm p,b} = 4.40^{+1.05}_{-1.03}$ Earth masses, while the ESPRESSO data converged to $M_{\rm p,b} = 6.85^{+1.29}_{-1.17}$ Earth masses. These are different at the 1.5σ level with, unsurprisingly, the mass as constrained by the full data set in between the values. We thus proceeded to check whether we could explain that difference.

The most obvious check would be to investigate the effect of changing the model. First, we looked at the inclusion of a third Keplerian in the model, given the periodicities present in the residuals of the global 2-Keplerian model. We ran additional models assuming 3-Keplerian signals, as explained in more detail in Section 7. The mass determinations of K2-111 b were well within 1σ, with 4.52 and 6.89 Earth masses from the HARPS-N and ESPRESSO data, respectively, and 5.67 Earth masses from the full data set. We have also run multiple models including a GP regression with a quasi-periodic kernel, as explained in detail in Section 6. The mass of K2-111 b stays well within 1σ of the 2-Keplerian model in all the cases, regardless of the number of included Keplerian signals additional to the GP. We conclude that changing the model (within reason) does not explain the modest discrepancy for the planet mass of K2-111 b.

Next, we looked at the sampling. Given the multiple periodicities present in the data, the near-3:1 resonance of these periods, and the unknown effects from stellar activity, sampling could be problematic. Both data sets have been sampled fairly differently. Within one season, the HARPS-N data have a median spacing of 1 d between measurements, with multiple dense series of observations. The ESPRESSO data have a median spacing of 5 d between measurements with individual observations being much more spaced out.

Inspired by the simulations from Rajpaul et al. (2017), we created synthetic data and used our real observing calendars and errors to extract the semi-amplitudes of the inserted signals. We have done so in an analytic manner to speed up computational time by keeping the periods fixed and analytically solving for the minimum chi-squared, weighted by the errors.

To create the synthetic data, we assumed circular orbits and used the periods and semi-amplitudes from the global fit of the full data with two circular Keplerians ($P_1 = 5.351962$ d, $K_1 = 2.17$ m/s and $P_2 = 15.679213$ d, $K_2 = 3.23$ m/s). We sampled uniformly over 50 different phases between $-\pi$ and π for both signals. The analytical solution was obtained assuming 1 m/s additional white noise, added in quadrature to the errors.[10] No noise was added to the individual data points meaning that if the data are sampled well, the semi-amplitudes should be extracted exactly as inserted. We used four different time series: the ESPRESSO observing calendar, the HARPS-N observing calendar, the combined calendar, and a uniform calendar using 154 data points sampled uniformly over the time span of the full data set and with uniform errors. We find that all observing calendars result in well-extracted semi-amplitudes, within 1 cm/s for both signals. The very different sampling of our data sets should thus not necessarily matter either.

As in Cloutier et al. (2019), we tried to identify any potentially anomalous points. For the fixed periods $P_1 = 5.3518$ d and $P_2 = 15.678$ d (corresponding to the two strongest signals in our data), we computed the BGLS periodogram probability and the associated fitted semi-amplitude and uncertainty (see Mortier et al. 2015; Mortier & Collier Cameron 2017, for details on the computation). We ran this 154 times, always leaving one data point out. We can thus compare how each data point affects the period probability and corresponding fit. From all data points, there is one data point that stands out. Leaving out that data point results in a fitted semi-amplitude that is different than all the other fitted semi-amplitudes (it is lower for both periods). We do note that, while an obvious outlier, the difference is just within the fitted semi-amplitude errors.

[10]Not adding white noise did not affect the outcome.

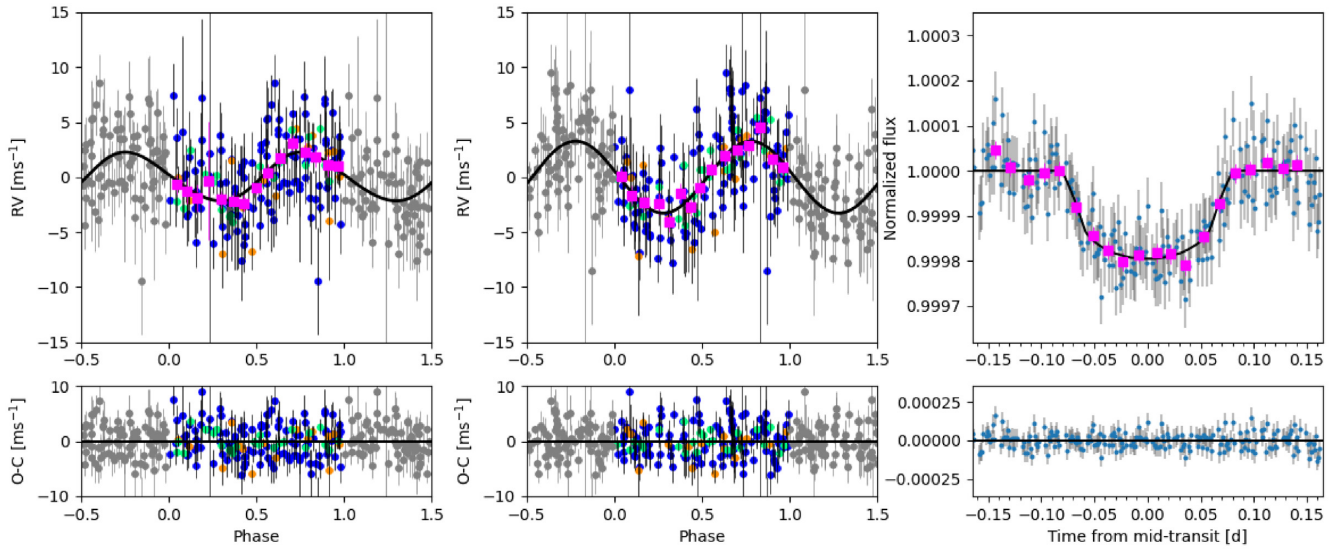

Figure 4. Solution from the global fit 2-Keplerian eccentric model. Left-hand panel: RV versus phase for K2-111 b (5.3518 d). Blue markers represent HARPS-N measurements, orange and green markers represent ESPRESSO 1 and 2 measurements, respectively, and magenta squares are the phase-binned data. The black curve represents the best model. White noise has been added to the errors. Middle panel: Same as the left-hand panel but for the second Keplerian at 15.678 d. Right-hand panel: transit of K2-111 b with blue points the *K2* data, magenta squares the phase-binned data, and the black line its best model. Bottom panels represent the residuals of each corresponding model.

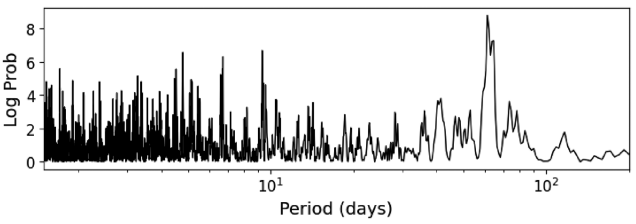

Figure 5. BGLS periodogram of the residual RVs after subtracting a 2-Keplerian eccentric model.

The data point is from the second set of ESPRESSO data at JDB = 2458821.675673 d.

We ran extra models excluding this data point, both for the ESPRESSO data set and the full data set. As expected, the planet mass of K2-111 b goes down but only marginally (from 5.29 to 5.11 Earth masses for the full data set). The one slightly anomalous ESPRESSO data point can thus not explain the difference either.

Given the different time span of the HARPS-N and ESPRESSO RV data, the small fitted mass difference could potentially arise from librating co-orbital bodies. We thus performed a co-orbital analysis for K2-111 b. We followed the theoretical framework described in Leleu et al. (2017) and subsequently applied in other observational works (e.g. Lillo-Box et al. 2018a, b; Toledo-Padrón et al. 2020) to constrain the presence of planet–mass co-orbital bodies. This framework introduces the parameter α in the usual RV equation, which corresponds to the mass ratio between the Trojan and the planet. If compatible with zero, the data are unable to constrain the presence of co-orbital bodies. If significantly different from zero and positive (negative), the signal contains hints for the presence of a mass imbalance at the L_5 (L_4) Lagrangian point (located at ± 60 degrees from the planet location and on the same orbital path in the restricted three-body problem). We assumed wide Gaussian priors on the planet parameters (using the 2-Keplerian circular model for simplicity). We find that $\alpha = 0.27^{+0.25}_{-0.21}$, which is compatible with zero at the 95 per cent confidence level. The distribution is, however, 1.3σ shifted towards positive values, indicating a possible mass imbalance at the L_5 location. The mass of a Trojan located exactly at this Lagrangian point and causing this imbalance would be $1.7^{+1.6}_{-1.3}$ $M_\oplus$, which allows us to discard at the 95 per cent confidence Trojans more massive than 4.5 $M_\oplus$ at L_5 and 0.4 $M_\oplus$ at L_4. Assuming coplanarity with the planet orbit, the median mass for this Trojan would imply a transit depth of $\sim$70 ppm at the limit of the photometric sensitivity from the *K2* data. An inspection of the phase-folded light curve does not show any dimming of this depth at the L_5 location or at any other location, although the photometric sensitivity, the possibility of libration, and mutual inclination with the planet's orbital plane leave the possibility of the co-orbital case still open.

Finally, we considered that the difference could be explained by unaccounted for effects of stellar variability. The WASP photometry and the ESPRESSO S-index both showed signs of periodicity in the vicinity of the transiting planet period. We have tried training a GP with a quasi-periodic kernel to the S-index data, but the posterior distributions were essentially always equal to the uniform prior distributions, even if we narrowed the 'rotation period' hyperparameter to be close to the peak seen in the BGLS periodogram. We found no obvious way of modelling possible stellar activity effects around the 5.35 -d period but hypothesize that it may be the explanation for the differences seen from both data sets.

From these tests, we conclude that the planet mass of K2-111 b is as accurate as we can confidently infer from the available data.

6 THE ORIGIN OF THE 15.678 DAY SIGNAL

For periodic signals in RV data, unrelated with known transiting planets, it is important to understand the origin of this signal. This can be mainly due to two things: a non-transiting planet or a signal created by stellar activity on the surface of the star (see e.g. Faria et al. 2020, for a good discussion on this).

Signals arising from stellar activity are often mimicked in activity indicators, such as the FWHM of the CCF or the S-index, even for

moderate or low-activity stars. A correlation coefficient between RVs and indicators may be lowered due to time shifts between the time series (see e.g. Santos et al. 2014; Collier Cameron et al. 2019), but similar periodicities are often seen in the data. For example, high-resolution observations from the Sun-as-a-star clearly show similar periodicity structure in the RVs and the indicators (Collier Cameron et al. 2019; Maldonado et al. 2019) around the rotation period and its harmonics while the correlation coefficients are lowered due to a 2-d time shift. It is therefore important that the 15.678-d signal appears so strongly in the RVs but is not seen in the BGLS periodograms of any indicator (Fig. 3). Overall, the indicators do not show strong periodicity at all while the RV signal in both the HARPS-N and ESPRESSO data is strong, consistent, and stable over time. This points to the 15.678-d signal being planetary.

Some photometry data we gathered do, in contrast with the spectral indicators, show more clear signs of periodicity around 30 d and its harmonic around 15 d. This could thus point to the signal seen in the RVs being stellar in origin. However, it is important to point out that, while there is some modest forested structure around 30 d in the HARPS-N RVs, the ESPRESSO RVs show no sign of a 30-d periodicity. If the 15.678- d signal is related to stellar activity, it would be surprising (but perhaps not impossible – see Nava et al. 2020) to see strong periodicity at the harmonic and none around the rotation period. Additionally, the *K2* data, while shorter in time span, firmly rule out variations greater than 500 ppm at this period.

Assuming that the 15.678-d signal may be stellar in origin, we used `PyORBIT` to model the RV data with a model including just the transiting planet, a GP with a quasi-periodic kernel (similar to what we did for the photometry in Section 3.5), and additional white noise. To speed up the computation, we modelled only the RV data and put priors on the parameters of the transiting planet based on a fit of the *K2* photometry only.

As a first run, we put additional priors on the rotation period, decay time-scale, and coherence scale based on the `PyORBIT` results of modelling all the photometry (see Section 3.5). The model converged to a reasonable solution. We compared the evidences of this model with a model of 2 Keplerians and white noise (also with a transiting planet prior and not using *K2* data). The 2-Keplerian model is decisively preferred with a Bayes factor exceeding 10^6.

We also ran `PyORBIT` while putting no priors on the kernel hyperparameters and allowing the rotation period to be below 100 d. The 2-Keplerian model is still preferred over this model, but the Bayes factor is only 16 now. The hyperparameters were constrained to $P_{\rm rot} = 62.67^{+0.07}_{-46.99}$ d, $P_{\rm dec} = 1594^{+289}_{-451}$ d, $h = 3.55^{+1.61}_{-0.85}$ m/s, and $w = 0.21^{+0.84}_{-0.05}$. It stands out that the decay time-scale goes to very high values, comparable with the time span of the RV data (which is 1590 d). The posterior distributions of the rotation period and coherence scale are both multimodal with peaks close to 60 and 15 d and corresponding coherence scales of 0.20 and 1, respectively. We thus ran three additional models where the rotation period hyperparameter was constrained to be around 15, 30, or 60 d. We saw the same result across all these models. The model evidences were lower than the 2-Keplerian model (with Bayes factors ranging from 4 to 247) and the decay time-scales converged to be higher than 1000 d.

It could, of course, still be the case that the periodicity between 15 and 16 d is a mixture of both stellar and planetary origin. We thus also ran a 2-Keplerian model with an additional quasi-periodic GP. Putting priors on the kernel hyperparameters from the photometry resulted in a good fit and an amplitude kernel hyperparameter of $h = 1.28 \pm 0.33$ m/s. The 2-Keplerian model without including a GP is still mildly preferred with a Bayes factor of 10. Importantly, the recovered mass for the 15.678 - Keplerian signal, if it were due to a planet, remains the same, within 1σ of all the other models we tried.

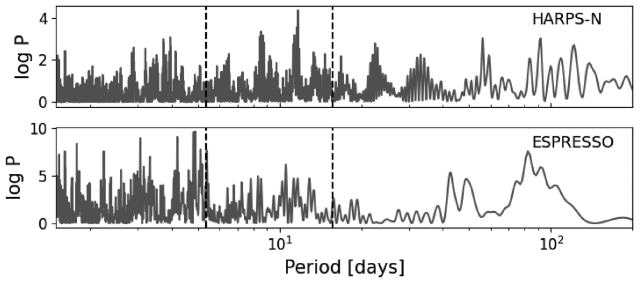

Figure 6. BGLS periodogram of the difference between the red and blue RVs – Log probability is plotted against period. Top plot is for HARPS-N data, bottom plot for ESPRESSO data. The vertical dashed lines represent the two strongest periodicities in the RVs.

Finally, we checked the coloured RVs as extracted from HARPS-N and ESPRESSO. Effects from stellar variability are not stable across wavelength while a signal arising from a planet should be the same regardless of the wavelength (e.g. Huélamo et al. 2008; Figueira et al. 2010; Reiners et al. 2010; Zechmeister et al. 2018). The red, green, and blue RVs from ESPRESSO show the same overall structure in the BGLS periodogram with peaks around the transiting planet period and around 15.678 d. For the HARPS-N coloured RVs, each set shows a different overall structure, but all three show strong probability around 15.678 d. We subtracted the red RVs from the blue RVs and plotted the BGLS periodogram of these residuals in Fig. 6 for each data set. Signals arising from planets should be fully removed in these residuals while stellar activity effects will remain. The probability for the 15.678-d signal is within the noise for both the HARPS-N and the ESPRESSO data making the planet hypothesis more likely than the activity hypothesis.

Interestingly, the strongest periodicities in the ESPRESSO coloured RV residuals are around 5 d and below. There may thus indeed be some excess signal in the transiting planet RV fit from the ESPRESSO data that comes from these short time-scale effects, as hypothesized in Section 5.

Given the highest, albeit sometimes marginal, evidence for the 2-Keplerian model, the high decay time-scale in the model with 1-Keplerian and a GP, the mass consistency for all 2-Keplerian models, and the consistency across wavelength, we conclude that the 15.678-d signal is stable, at least over the time-scale of the data, and it points towards the signal being planetary in origin rather than stellar. We use K2-111 c for this candidate planet for the remainder of this work.

We checked the *K2* light curve for signs of K2-111 c. The light curve, phase-folded with the orbital period and phase mentioned in Table 4, is shown in Fig. 7. Assuming the probabilistic mass–radius relation of Chen & Kipping (2017), K2-111 c is expected to have a radius of 3.37 $R_\oplus$. This would result in a transit depth of 0.0006. If this planet would transit, we would be able to easily detect it in the *K2* light curve. With no points lower than 0.9997 in the light curve, it is clear that K2-111 c does not transit. Assuming co-planarity between the two planets, the impact parameter of K2-111 c would be 1.25, indicating that we would not expect this second planet to transit.

Both planets orbit K2-111 in near 3:1 mean–motion resonance. This could induce transit timing variations (TTVs) for the transiting planet K2-111 b. We checked for this by fitting for each transit separately. Since the star was observed in long cadence, the amount of data points in each individual transit is low. We thus kept the depth of each transit fixed to the value obtained from the global fit and

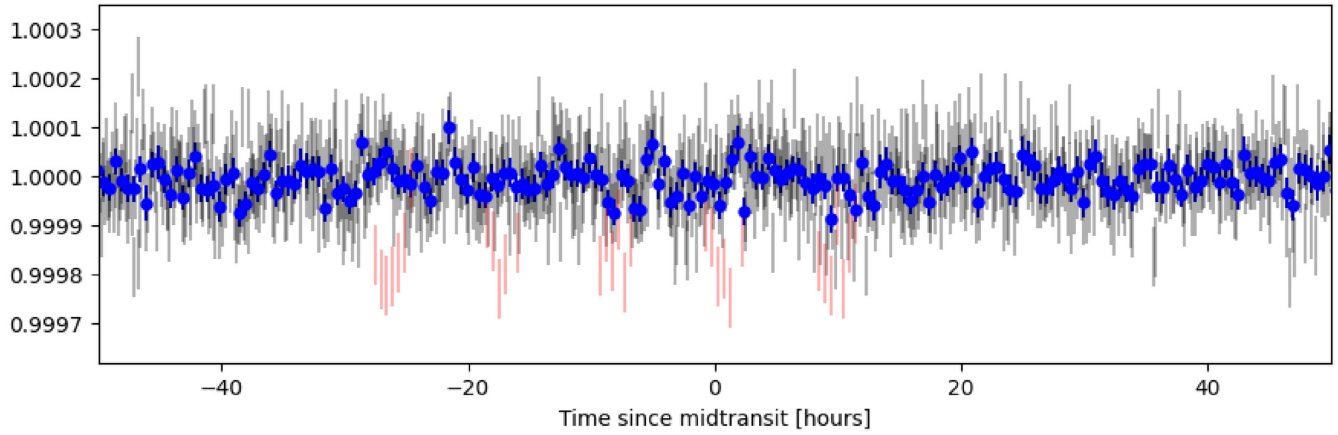

Figure 7. Flux versus time of the *K2* light curve, phase-folded with the orbital period and phase of K2-111 c. Blue dots are binned data, binned over 30 min. Grey and red errors are shown from the unbinned data where the red errors are the photometric points inside the transit of K2-111 b. The expected transit depth of K2-111 c, assuming a mass–radius relation from Chen & Kipping (2017), is 0.0006, well below the lowest point in the figure.

allowed only the central time of transit to vary. All transits occurred on the predicted time from a constant period, fully consistent with a null result on TTV; however, as expected, errors on the TTVs are quite large, on the order of 10 min. We used REBOUND[11] (Rein & Liu 2012), an *N*-body integrator, to estimate the expected TTV variations, given our orbital solution. We found that the maximum expected amplitude of TTV variations would be 2 min, well below our precision and fully consistent with our values being close to zero.

7 ADDITIONAL SIGNALS IN THE DATA

As mentioned in Section 4, there is some periodicity left around 60 d in the residuals of the global 2-Keplerian model. We thus fitted the RV data and *K2* photometry with a 3-Keplerian model, which converged to a good solution. The 3-Keplerian model is slightly preferred, but only with a Bayes factor of 46, not enough to decisively say the 3-Keplerian model is more likely. From Fig. 6, we can see that neither data set shows strong signs of chromaticity for periods between 60 and 70 d. If the third Keplerian were due to a planet, it would have a minimum mass of seven Earth masses. The masses of K2-111 b and K2-111 c do not change within 1σ of the 2-Keplerian solution.

When looking more closely at the solution of this 3-Keplerian model, the posterior distribution for the period of the third Keplerian is bimodal with a solution around 61.5 d and one around 64.5 d. These two periods are likely aliases from each other, due to the time span of the data. Both solutions have similar probabilities and similar orbital parameters, and it is unclear how to favour one over the other. Judging solely from phase coverage, we can say that the Keplerian solution around 61.5 d is less well sampled in phase space than the 64.5 d solution.

Interestingly, the BGLS periodogram of the residuals from the 2-Keplerian model including a GP shows less probability around 60 d. We thus also ran a 3-Keplerian model including a GP. The model evidence was only a bit lower than the 2-Keplerian model. Overall, the orbital parameters of all three Keplerians were similar than for the model without the GP. The posterior distribution of the period is, however, no longer bimodal and only the 61.5-d, less well-sampled, solution is found.

[11] http://github.com/hannorein/rebound

It would not be surprising if there were more planets in this system, in addition to K2-111 b and K2-111 c. The current data, however, do not allow us to draw strong conclusions about the existence of these additional planets.

8 DISCUSSION AND CONCLUSION

In this work, we have confirmed the presence of the transiting planet K2-111 b. We have refined the planetary parameters, especially the planetary mass. The planetary radius, $1.82^{+0.11}_{-0.09}$ Earth radii, is significant to 20σ. Our fitted planet radius is marginally lower than the one reported in Fridlund et al. (2017) ($R_\mathrm{p} = 1.9 \pm 0.2\,\mathrm{R}_\oplus$) but twice as precise. This is almost solely due to the more precise and accurate stellar radius, possible with the *Gaia* DR2 parallax measurement. We fitted the planet mass of K2-111 b to $5.29^{+0.76}_{-0.77}$ Earth masses, significant to almost 7σ. Our fitted value is about three Earth masses lower than the mass reported by Fridlund et al. (2017), but we note that they had measured only the planet mass to within 2σ ($M_\mathrm{p} = 8.6 \pm 3.9\,\mathrm{M}_\oplus$).

We also announce the presence of an additional non-transiting planet in this system, K2-111 c, at 15.678 d with a minimum mass of 11.3 ± 1.1 Earth masses. While not confirmed with an independent technique, we have shown in Section 6 that the detected RV signal is unlikely to have arisen from stellar surface phenomena.

We have used two RV data sets that are qualitatively equal, with more data points from HARPS-N and higher precision from ESPRESSO. These data sets independently detected the two planets, with mass measurements significant to at least 4σ, though discrepant at the 1.5σ level. Combining these two exquisite data sets made the detections much more significant and strengthened the planet hypothesis for the 15.678-d signal, now called K2-111 c.

Fridlund et al. (2017) had hypothesized the presence of a more massive object with a period longer than 120 d in their work from a fitted linear trend in their model. Neither the HARPS-N nor the ESPRESSO data show any signs of a long-term trend or indicate the presence of such a massive outer companion. We think that the appearance of a linear trend in the data used by Fridlund et al. (2017) was the result of the short data time span and very sparse sampling for this resonant planetary system. The period of K2-111 c is a bit less than three times the period of the transiting planet making these two planets orbit in near-3:1 resonance.

We do see signs of a potential additional super-Earth with a period around 61.5 d and a minimum mass of seven Earth masses. The current data set is not sufficient to draw conclusions about the nature of this signal. It is, however, interesting to note that, if this is indeed a planet, the period would be about four times the period of K2-111 c, making the three planets fit nicely in a near-resonant chain.

Given the near-3:1 resonance of the two planets in this system, we investigated the dynamical stability. As also illustrated in Fridlund et al. (2017), for the estimated mass of K2-111 c, we would expect the system to be stable unless the eccentricity exceeded $e \sim 0.3$ (Petrovich 2015). To check this, we ran a small suite of *N*-body simulations using MERCURY6.2 (Chambers 1999) with the Bulirsch–Stoer integrator. We set the orbital parameters and planet masses by randomly sampling from the ranges presented in Table 4. These simulations indicate that the planetary system is indeed stable on long time-scales (well beyond 10^8 yr).

We also used these simulations to check if the periodicity at around 60 d in the residuals of the global 2-Keplerian model could be due to some kind of resonant interaction between the two inner planets. From five of the *N*-body simulations, we considered a period of 1000 d and randomly extracted ∼200 stellar RVs. We then added noise to these RVs with a magnitude similar to that of the jitter presented in Table 4 and assumed that the uncertainties were similar to those presented in Table 1.

We first used PyORBIT to check that it would recover the two known planets in these synthetic data. This was the case with a similar precision to that presented in Table 4. We then used PyORBIT to check if it could recover a statistically significant three-planet solution, assuming that the third planet has a period $P > 30$ d. All of these analyses recovered the two known planets, but none converged on a three-planet solution. Therefore, it seems unlikely that the long-period signal is due to a resonant interaction between the two inner planets.

The K2-111 system is also intriguing as the host star, with an age at least older than 10 Gyr, is among the oldest stars in the Universe. Given this old age, it is possible that the planetary orbits, and especially the inner one, would have circularized (see e.g. Goldreich & Soter 1966; Jackson, Greenberg & Barnes 2008). This is in line with the eccentricities being fully consistent with zero. The orbits are in near mean–motion resonance, which could pump the eccentricities of the orbits as well, impeding tidal circularization (see e.g. Beust & Morbidelli 1996). Indeed, there are other examples of close-in planets on eccentric orbits around very old stars (e.g. Motalebi et al. 2015; Mortier et al. 2016).

Not much is known about planetary systems around the very oldest stars and the history of their formation. It is therefore crucial that we study these systems, as also pointed out by Fridlund et al. (2017). We checked the NASA Exoplanet Archive.[12] Roughly half of the >4000 planets listed in the archive mention a stellar age for the planet host. Only 57 of these, orbiting 39 different stars, have a stellar host age greater than 10 Gyr, including K2-111. We do caution that most stellar ages are badly constrained. When we take into account that our host star is also iron-poor and select only those systems with sub-solar overall metallicity, there are only 22 planets left, orbiting 15 stars, with a wide variety of orbital and planetary parameters.

Fig. 8 shows the mass–radius diagram for K2-111 b together with all small planets ($R_p < 4\,R_\oplus$) where a mass measurement is known with a significance better than 3σ. K2-111 b sits in a region between the 50 per cent H_2O and 100 per cent $MgSiO_3$ composition lines (Zeng & Sasselov 2013; Zeng, Sasselov & Jacobsen 2016), with a bulk density slightly lower than the Earth. There are no obvious trends noticeable with stellar age, which could be due to low-number statistics.

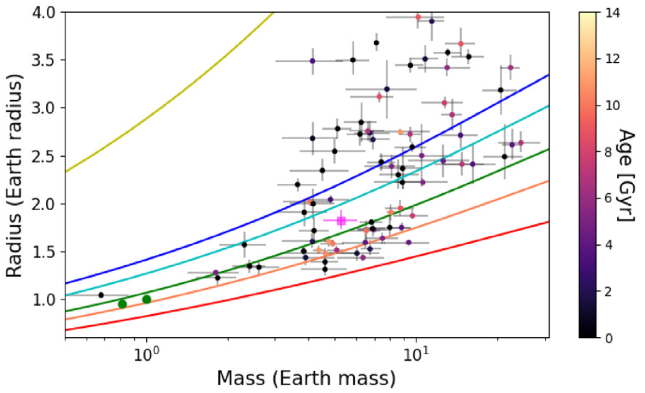

Figure 8. Mass–radius diagram of all planets smaller than $4\,R_\oplus$ with a mass measurement significance better than 3σ (using data from the NASA exoplanet archive accessed 2020 June 11). The points are colour-coded according to their stellar host ages (in case no age was determined, the point is black). The green dots bottom left represent Venus and Earth, respectively. The solid lines show planetary interior models for different compositions, top to bottom: Cold H_2/He, 100 per cent H_2O, 50 per cent H_2O, 100 per cent $MgSiO_3$, 50 per cent Fe, and 100 per cent Fe. The larger magenta square represents K2-111 b.

8.1 Interior structure of K2-111 b

The host star, K2-111, is iron-poor. This in itself is interesting as there are only a handful of small planets around iron-poor stars that have their radius and mass both measured. More interestingly, however, is the significant alpha-enhancement of K2-111. The ratios between iron, magnesium, and silicon are different to the solar ratios. As these elements are the core building blocks for a planet's core and mantle, the difference in these ratios is important as this could affect the interior structure of the small planets around K2-111.

Using the stellar chemical composition, we can infer the mass fraction of the planet building blocks in the K2-111 system, assuming that the stellar composition is a good proxy for the disc composition at the time of planet formation. We can use our obtained chemical abundances from the spectra for this purpose. We followed the procedure described in Santos et al. (2015) and Santos et al. (2017), which uses a simple stoichiometric model and chemical abundances of Fe, Mg, Si, C, and O to predict expected iron and silicates mass fractions of the planet building blocks. For K2-111, we find that the expected mass fractions of the iron and silicates building blocks are 21 per cent and 79 per cent, respectively. The iron mass fraction is, as expected for this old, alpha-enhanced star, significantly lower than the iron mass fraction of the solar planet building blocks (Santos et al. 2017).

With both a precise planetary mass and radius for K2-111 b, we can go a step further and perform a more detailed modelling of the stellar, planetary, and orbital characteristics to infer the possible interior structure of the transiting planet. The methodology we used is described in Alibert et al. (2020 - submitted) and is based on the models used by Dorn et al. (2015) and Dorn et al. (2017). The physical model has been improved since those works, e.g. by using a

[12] https://exoplanetarchive.ipac.caltech.edu – accessed on 2020 June 11.

new equation of state for the water layer (Haldemann et al. 2020). The gas envelope is treated using the model of Lopez & Fortney (2014), which gives the thickness of the gas envelope as a function of the age, planetary mass, etc. We neglect in this analysis the effect of the gas envelope on the radius of the solid part. The analysis is now also done using neural networks exploring the probability distributions of the internal structure parameters. We refer to Alibert et al. (2020 - submitted) for more details.

The data going into the model are the stellar mass, radius, effective temperature, and age, as well as the chemical abundances of Fe, Mg, Si, and the planetary mass, radius, and period. The posterior distributions of the relevant internal structure parameters are shown in Fig. S5 in the online supplementary material. We find that K2-111 b has a small gas envelope ($\sim$0.01 $M_\oplus$ and 0.1 $R_\oplus$ of gas). This shows that neglecting the compression effect of the gas envelope on to the planetary interior, which the model assumes, is perfectly justified in our case. The planet has an iron core with a mass fraction of around 10 per cent (much smaller than the Earth), a big silicate mantle (up to more than 80 per cent of the planet mass could be in the mantle), while the water layer is less well constrained (the posterior distribution has a slight preference for a small mass fraction). This result is again in agreement with the star being iron-poor and is qualitatively similar to the results from the simple stoichiometry model.

Due to the star being very old and the planet orbiting relatively close to the star, it is likely that an 0.1 $R_\oplus$ H/He gas envelope around K2-111 b did not survive due to photo-evaporation. When we do not allow a gas envelope to be present in our model, this results in a very similar solution with a small iron core, a large silicate mantle, and an unconstrained but likely small volatile layer. This is unsurprising, given the gas envelope was found to be small and only 0.01 $M_\oplus$ in the original model.

Finally, we explored whether the planetary and stellar parameters could be consistent with a truly terrestrial model where the planet interior structure is composed of only an iron core and a silicate mantle. We find that the stellar and planetary characteristics are consistent, within 2σ, with such a terrestrial two-layer model for K2-111 b. The posterior distributions of these internal structure parameters are shown in Fig. S6 in the online supplementary material. The iron core mass fraction in this scenario is 13 per cent, still significantly less than the Earth. The slightly higher mass as derived from the ESPRESSO data alone could be favoured for this terrestrial two-layer model and make it more consistent than 2σ. If we allowed a gas envelope with the two-layer model, we found that the gas envelope was again fitted to very small values, ruling out a large gas envelope that could potentially be stable around a terrestrial planet.

We caution that these results are model-dependent and that more models with various physical ingredients should be explored, but K2-111 b could be an actual terrestrial planet, though with a much lower core mass fraction than the Earth, compatible with its host's stellar composition. The small core mass fraction is a feature likely shared by other planets around thick disc or halo stars, given their reduced iron mass fractions compared to planets around thin disc stars (see e.g. Santos et al. 2017). Recently, Michel et al. (2020) showed that solid planets around thick disc or halo stars have a larger radii than planets around thin disc stars.

Planet formation and evolution theories improve by the discovery of more planetary systems around a variety of stars. To understand the small details of every aspect of planet formation and evolution, it is of the utmost importance that we keep studying and characterizing planetary systems in a wide parameter space, both for the stars and the planets. Precisely and accurately characterizing systems like K2-111 will refine our knowledge of planetary systems in the Galaxy.

ACKNOWLEDGEMENTS

We thank the referee for a constructive report. We thank Josh Briegal and João Faria for helpful discussions.

AMo acknowledges support from the senior Kavli Institute Fellowships. MRZO acknowledges financial support from the Spanish Ministry of Science and Innovation (MICINN) AYA2016-79425-C3-2-P. JIGH acknowledges financial support from the Spanish MICINN under the 2013 Ramón y Cajal programme RYC-2013-14875. ASM acknowledges financial support from the Spanish MICINN under the 2019 Juan de la Cierva Programme. JIGH, ASM, RR, and CAP acknowledge financial support from the Spanish MICINN AYA2017-86389-P. ACC acknowledges support from the Science and Technology Facilities Council (STFC) consolidated grant number ST/R000824/1. CAW would like to acknowledge support from UK STFC grant ST/P000312/1. PF was supported by MCTES through national funds (PIDDAC, PTDC/FIS-AST/32113/2017). MP acknowledges financial support from the ASI-INAF agreement n. 2018-16-HH.0. YA and JH acknowledge the Swiss National Science Foundation (SNSF) for supporting research through the SNSF grant 200020_192038. VA, EDM, SS, SCCB, and ODSD acknowledge support from Fundação para a Ciência e a Tecnologia (FCT) through Investigador FCT contracts IF/00650/2015/CP1273/CT0001, IF/00849/2015/CP1273/CT0003, IF/00028/2014/CP1215/CT0002, IF/01312/2014/CP1215/CT0004, and DL 57/2016/CP1364/CT0004. This work was supported by FCT through national funds and by FEDER through COMPETE2020 – Programa Operacional Competitividade e Internacionalização by these grants: UID/FIS/04434/2019; UIDB/04434/2020; UIDP/04434/2020; PTDC/FIS-AST/32113/2017 & POCI-01-0145-FEDER-032113; PTDC/FIS-AST/28953/2017 & POCI-01-0145-FEDER-028953; and PTDC/FIS-AST/28987/2017 & POCI-01-0145-FEDER-028987. Parts of this work have been supported by the National Aeronautics and Space Administration under grant no. NNX17AB59G issued through the Exoplanets Research Program. Part of this work has been carried out within the framework of the NCCR PLanetS supported by the SNSF. The INAF authors acknowledge financial support of the Italian Ministry of Education, University, and Research with PRIN 201278X4FL and the 'Progetti Premiali' funding scheme. FAP and CL would like to acknowledge the SNSF for supporting research with ESPRESSO through the SNSF grant nos. 140649, 152721, 166227, and 184618 and with HARPS-N through the SNSF grant nos. 140649, 152721, 166227, and 184618. The ESPRESSO Instrument Project was partially funded through SNSF's FLARE Programme for large infrastructures. The HARPS-N Instrument Project was partially funded through the Swiss ESA-PRODEX Programme. This publication was made possible through the support of a grant from the John Templeton Foundation. The opinions expressed in this publication are those of the authors and do not necessarily reflect the views of the John Templeton Foundation. This project has received funding from the European Research Council (ERC) under the European Union's Horizon 2020 research and innovation programme (project FOUR ACES; grant agreement no. 724427).

This research has made use of the SIMBAD data base, operated at CDS, Strasbourg, France, NASA's Astrophysics Data System, and the NASA Exoplanet Archive, which is operated by the California Institute of Technology, under contract with the National Aeronautics and Space Administration under the Exoplanet Exploration Program. Based on Guaranteed Time Observations collected at the European Southern Observatory under ESO programmes 1102.C-0744, 112.C-0958, and 1104.C-0350 by the ESPRESSO Consortium. Based on

observations made with the Italian Telescopio Nazionale Galileo (TNG) operated on the island of La Palma by the Fundacion Galileo Galilei of the INAF (Istituto Nazionale di Astrofisica) at the Spanish Observatorio del Roque de los Muchachos of the Instituto de Astrofisica de Canarias. The HARPS-N project has been funded by the Prodex Program of the Swiss Space Office (SSO), the Harvard University Origins of Life Initiative (HUOLI), the Scottish Universities Physics Alliance (SUPA), the University of Geneva, the Smithsonian Astrophysical Observatory (SAO), and the Italian National Astrophysical Institute (INAF), the University of St Andrews, Queen's University Belfast, and the University of Edinburgh. We acknowledge the University of Warwick for running the WASP Data Centre. This paper includes data collected by the *K2* mission. Funding for the *K2* mission is provided by the NASA Science Mission directorate. Some of the data presented in this paper were obtained from the Mikulski Archive for Space Telescopes (MAST). STScI is operated by the Association of Universities for Research in Astronomy, Inc., under NASA contract NAS5-26555. Support for MAST for non-*HST* data is provided by the NASA Office of Space Science via grant NNX13AC07G and by other grants and contracts. This work has made use of data from the European Space Agency (ESA) mission *Gaia* (https://www.cosmos.esa.int/gaia), processed by the *Gaia* Data Processing and Analysis Consortium (DPAC, https://www.cosmos.esa.int/web/gaia/dpac/consortium). Funding for the DPAC has been provided by national institutions, in particular, the institutions participating in the *Gaia* Multilateral Agreement.

DATA AVAILABILITY

All underlying data are either available in the appendix/online supporting material or will be available via VizieR at CDS.

REFERENCES

Adibekyan V. Z., Delgado Mena E., Sousa S. G., Santos N. C., Israelian G., González Hernández J. I., Mayor M., Hakobyan A. A., 2012b, A&A, 547, A36
Adibekyan V. Z., Sousa S. G., Santos N. C., Delgado Mena E., González Hernández J. I., Israelian G., Mayor M., Khachatryan G., 2012a, A&A, 545, A32
Asplund M., Grevesse N., Sauval A. J., Scott P., 2009, ARA&A, 47, 481
Bailer-Jones C. A. L., Rybizki J., Fouesneau M., Mantelet G., Andrae R., 2018, AJ, 156, 58
Baranne A. et al., 1996, A&AS, 119, 373
Belokurov V. et al., 2020, MNRAS, 496, 1922
Bertran de Lis S., Delgado Mena E., Adibekyan V. Z., Santos N. C., Sousa S. G., 2015, A&A, 576, A89
Beust H., Morbidelli A., 1996, Icarus, 120, 358
Borucki W. J. et al., 2010, Science, 327, 977
Buchhave L. A. et al., 2012, Nature, 486, 375
Buchhave L. A. et al., 2014, Nature, 509, 593
Chambers J. E., 1999, MNRAS, 304, 793
Chen J., Kipping D., 2017, ApJ, 834, 17
Cincunegui C., Díaz R. F., Mauas P. J. D., 2007, A&A, 469, 309
Cloutier R. et al., 2019, A&A, 621, A49
Collier Cameron A. et al., 2006, MNRAS, 373, 799
Collier Cameron A. et al., 2019, MNRAS, 487, 1082
Cosentino R., et al., 2012, in McLean Ian S., Ramsay Suzanne K., Takami Hideki, eds, Proc. SPIE Conf. Ser. Vol. 8446, Ground-based and Airborne Instrumentation for Astronomy IV, SPIE, Bellingham. p. 84461V
Cutri R. M. et al., 2003, VizieR Online Data Catalog II/246
Cutri R. M. et al., 2014, VizieR Online Data Catalog. II/328
Delgado Mena E., Tsantaki M., Adibekyan V. Z., Sousa S. G., Santos N. C., González Hernández J. I., Israelian G., 2017, A&A, 606, A94
Delgado Mena E. et al., 2019, A&A, 624, A78
Dorn C., Khan A., Heng K., Connolly J. A. D., Alibert Y., Benz W., Tackley P., 2015, A&A, 577, A83
Dorn C., Venturini J., Khan A., Heng K., Alibert Y., Helled R., Rivoldini A., Benz W., 2017, A&A, 597, A37
Dotter A., 2016, ApJS, 222, 8
Dotter A., Chaboyer B., Jevremović D., Kostov V., Baron E., Ferguson J. W., 2008, ApJS, 178, 89
Dubber S. C. et al., 2019, MNRAS, 490, 5103
Dumusque X. et al., 2014, ApJ, 789, 154
Dumusque X. et al., 2017, A&A, 598, A133
Eastman J., Gaudi B. S., Agol E., 2013, PASP, 125, 83
Egeland R., Soon W., Baliunas S., Hall J. C., Pevtsov A. A., Bertello L., 2017, ApJ, 835, 25
Faria J. P. et al., 2020, A&A, 635, A13
Feroz F., Hobson M. P., Cameron E., Pettitt A. N., 2019, Open J. Astrophys., 2, 10
Figueira P. et al., 2010, A&A, 511, A55
Fridlund M. et al., 2017, A&A, 604, A16
Fulton B. J. et al., 2017, AJ, 154, 109
Gaia Collaboration, 2016, A&A, 595, A1
Gaia Collaboration, 2018, A&A, 616, A1
Goldreich P., Soter S., 1966, Icarus, 5, 375
Gomes da Silva J., Santos N. C., Bonfils X., Delfosse X., Forveille T., Udry S., 2011, A&A, 534, A30
Grunblatt S. K., Howard A. W., Haywood R. D., 2015, ApJ, 808, 127
Haldemann J., Alibert Y., Mordasini C., Benz W., 2020, preprint (arXiv:2009.10098)
Haywood M., 2009, ApJ, 698, L1
Haywood R. D. et al., 2014, MNRAS, 443, 2517
Hinkel N. R., Unterborn C. T., 2018, ApJ, 853, 83
Hojjatpanah S. et al., 2020, A&A, 639, A35
Howell S. B. et al., 2014, PASP, 126, 398
Huélamo N. et al., 2008, A&A, 489, L9
Jackson B., Greenberg R., Barnes R., 2008, ApJ, 678, 1396
Javoy M. et al., 2010, Earth Planet. Sci. Lett., 293, 259
Johnson D. R. H., Soderblom D. R., 1987, AJ, 93, 864
Kass R. E., Raftery A. E., 1995, J. Am. Stat. Assoc., 90, 773
Kochanek C. S. et al., 2017, PASP, 129, 104502
Kreidberg L., 2015, PASP, 127, 1161
Kurucz R., 1993, ATLAS9 Stellar Atmosphere Programs and 2 km/s grid. Kurucz CD-ROM No. 13. Mass.: Smithsonian Astrophysical Observatory, Cambridge, p. 13
Leleu A., Robutel P., Correia A. C. M., Lillo-Box J., 2017, A&A, 599, L7
Lillo-Box J., Barrado D., Figueira P., Leleu A., Santos N. C., Correia A. C. M., Robutel P., Faria J. P., 2018a, A&A, 609, A96
Lillo-Box J. et al., 2018b, A&A, 618, A42
Lopez E. D., Fortney J. J., 2014, ApJ, 792, 1
López-Morales M. et al., 2016, AJ, 152, 204
Malavolta L., 2016, Astrophysics Source Code Library, record ascl:1612.008
Malavolta L., Lovis C., Pepe F., Sneden C., Udry S., 2017b, MNRAS, 469, 3965
Malavolta L. et al., 2016, A&A, 588, A118
Malavolta L. et al., 2017a, AJ, 153, 224
Malavolta L. et al., 2018, AJ, 155, 107
Maldonado J. et al., 2019, A&A, 627, A118
Mamajek E. E., Hillenbrand L. A., 2008, ApJ, 687, 1264
Mayor M., Queloz D., 1995, Nature, 378, 355
Mayor M. et al., 2003, Messenger, 114, 20
Mazeh T., Tamuz O., Zucker S., 2007, in Afonso C., Weldrake D., Henning T., eds, ASP Conf. Ser. Vol. 366, Transiting Extrapolar Planets Workshop. Astron. Soc. Pac., San Francisco, p. 119
Michel A., Haldemann J., Mordasini C., Alibert Y., 2020, A&A, 639, A66
Mortier A., Collier Cameron A., 2017, A&A, 601, A110
Mortier A., Faria J. P., Correia C. M., Santerne A., Santos N. C., 2015, A&A, 573, A101

Mortier A., Santos N. C., Sousa S. G., Fernandes J. M., Adibekyan V. Z., Delgado Mena E., Montalto M., Israelian G., 2013, A&A, 558, A106
Mortier A., Sousa S. G., Adibekyan V. Z., Brandão I. M., Santos N. C., 2014, A&A, 572, A95
Mortier A. et al., 2016, A&A, 585, A135
Morton T. D., 2015, Astrophysics Source Code Library, record ascl:1503.010
Motalebi F. et al., 2015, A&A, 584, A72
Moutou C. et al., 2013, Icarus, 226, 1625
Nava C., López-Morales M., Haywood R. D., Giles H. A. C., 2020, AJ, 159, 23
Nissen P. E., Christensen-Dalsgaard J., Mosumgaard J. R., Silva Aguirre V., Spitoni E., Verma K., 2020, A&A, 640, A81
Noyes R. W., Hartmann L. W., Baliunas S. L., Duncan D. K., Vaughan A. H., 1984a, ApJ, 279, 763
Noyes R. W., Weiss N. O., Vaughan A. H., 1984b, ApJ, 287, 769
Pels G., Oort J. H., Pels-Kluyver H. A., 1975, A&A, 43, 423
Pepe F. et al., 2002, Messenger, 110, 9
Pepe F. et al., 2014, Astron. Nachr., 335, 8
Pepe F. et al., 2020, preprint (arXiv:2010.00316)
Petrovich C., 2015, ApJ, 808, 120
Pollacco D. et al., 2006, Ap&SS, 304, 253
Rajpaul V., Aigrain S., Osborne M. A., Reece S., Roberts S., 2015, MNRAS, 452, 2269
Rajpaul V., Buchhave L. A., Aigrain S., 2017, MNRAS, 471, L125
Reddy B. E., Lambert D. L., Allende Prieto C., 2006, MNRAS, 367, 1329
Reiners A., Bean J. L., Huber K. F., Dreizler S., Seifahrt A., Czesla S., 2010, ApJ, 710, 432
Rein H., Liu S. F., 2012, A&A, 537, A128
Ricker G. R. et al., 2015, J. Astron. Telesc. Instrum. Syst., 1, 014003
Santos N. C. et al., 2014, A&A, 566, A35
Santos N. C. et al., 2015, A&A, 580, L13
Santos N. C. et al., 2017, A&A, 608, A94
Shappee B. J. et al., 2014, ApJ, 788, 48
Sneden C. A., 1973, PhD thesis, The University of Texas at Austin
Sousa S. G., 2014, in Niemczura Ewa, Smalley Barry, Pych Wojtek, eds. Determination of Atmospheric Parameters of B-, A-, F- and G-Type Stars.: ARES + MOOG: A Practical Overview of an Equivalent Width (EW) Method to Derive Stellar Parameters, Springer International Publishing , Cham. p. 297
Sousa S. G., Santos N. C., Israelian G., Lovis C., Mayor M., Silva P. B., Udry S., 2011, A&A, 526, A99+
Sousa S. G. et al., 2015, A&A, 576, A94
Suárez Mascareño A., Rebolo R., González Hernández J. I., Esposito M., 2017, MNRAS, 468, 4772
Suárez Mascareño A. et al., 2020, A&A, 639, A77
Thiabaud A., Marboeuf U., Alibert Y., Leya I., Mezger K., 2015, A&A, 580, A30
Toledo-Padrón B. et al., 2020, A&A, 641, A92
Torres G., Fischer D. A., Sozzetti A., Buchhave L. A., Winn J. N., Holman M. J., Carter J. A., 2012, ApJ, 757, 161
Vanderburg A., Johnson J. A., 2014, PASP, 126, 948
Vanderburg A. et al., 2016, ApJS, 222, 14
Van Eylen V., Agentoft C., Lundkvist M. S., Kjeldsen H., Owen J. E., Fulton B. J., Petigura E., Snellen I., 2018, MNRAS, 479, 4786
Weiss L. M. et al., 2016, ApJ, 819, 83
Zacharias N., Finch C. T., Girard T. M., Henden A., Bartlett J. L., Monet D. G., Zacharias M. I., 2012, VizieR Online Data Catalog. I/322A
Zechmeister M. et al., 2018, A&A, 609, A12
Zeng L., Sasselov D., 2013, PASP, 125, 227
Zeng L., Sasselov D. D., Jacobsen S. B., 2016, ApJ, 819, 127
Zeng L. et al., 2017, in 48th Lunar and Planetary Science Conference. p. 1576

SUPPORTING INFORMATION

Supplementary data are available at *MNRAS* online.

Figure S1. Full time series of the WASP and ASAS photometry time series.
Figure S2. Full time series of the RVs and the indicators.
Figure S3. Corner plot of the planetary fitting parameters of the adopted 2-Keplerian model.
Figure S4. Corner plot of the stellar and instrumental fitting parameters of the adopted 2-Keplerian model.
Figure S5. Corner plot of the interior structure parameters for the model including a gas envelope and a water layer.
Figure S6. Corner plot of the interior structure parameters for the model with only an iron core and a silicate mantle.
Table S1. K2-111 system parameters from combined circular fit.
Table S2. Radial velocities and activity indicators for K2-111. The full table can also be found online.

Please note: Oxford University Press is not responsible for the content or functionality of any supporting materials supplied by the authors. Any queries (other than missing material) should be directed to the corresponding author for the article.

[1]*Astrophysics Group, Cavendish Laboratory, University of Cambridge, J.J. Thomson Avenue, Cambridge CB3 0HE, UK*
[2]*Kavli Institute for Cosmology, University of Cambridge, Madingley Road, Cambridge CB3 0HA, UK*
[3]*Centro de Astrobiología (CSIC-INTA), Crta. Ajalvir km 4, E-28850 Torrejón de Ardoz, Madrid, Spain*
[4]*Dip. di Fisica e Astronomia Galileo Galilei, Università di Padova, Vicolo dell'Osservatorio 2, I-35122, Padova, Italy*
[5]*Physics Institute, University of Bern, Sidlerstrasse 5, CH-3012 Bern, Switzerland*
[6]*SUPA, Institute for Astronomy, Royal Observatory, University of Edinburgh, Blackford Hill, Edinburgh EH93HJ, UK*
[7]*Centre for Exoplanet Science, University of Edinburgh, Edinburgh, UK*
[8]*Department of Astronomy, The University of Texas at Austin, 2515 Speedway, Stop C1400, Austin, TX 78712, USA*
[9]*Instituto de Astrofísica de Canarias (IAC), Calle Vía Láctea s/n, E-38205 La Laguna, Tenerife, Spain*
[10]*Departamento de Astrofísica, Universidad de La Laguna (ULL), E-38206 La Laguna, Tenerife, Spain*
[11]*DTU Space, National Space Institute, Technical University of Denmark, Elektrovej 328, DK-2800 Kgs. Lyngby, Denmark*
[12]*Instituto de Astrofísica e Ciências do Espaço, Universidade do Porto, CAUP, Rua das Estrelas, P-4150-762, Porto, Portugal*
[13]*Centro de Astrofísica da Universidade do Porto, Rua das Estrelas, P-4150-762 Porto, Portugal*
[14]*Departamento de Física e Astronomia, Faculdade de Ciências, Universidade do Porto, Rua Campo Alegre, P-4169-007, Porto, Portugal*
[15]*Center for Astrophysics | Harvard & Smithsonian, 60 Garden Street, Cambridge, MA 02138 USA*
[16]*Observatoire Astronomique de l'Université de Genève, Chemin des Maillettes 51, Sauverny, CH-1290, Switzerland*
[17]*INAF, Osservatorio Astronomico di Palermo, Piazza del Parlamento 1, I-90134 Palermo, Italy*
[18]*INAF, Osservatorio Astrofisico di Torino, via Osservatorio 20, I-10025 Pino Torinese, Italy*
[19]*Fundación G. Galilei, INAF (Telescopio Nazionale Galileo), Rambla J. A. Fernández Pérez 7, E-38712 Breña Baja, La Palma, Spain*
[20]*Instituto de Astrofísica e Ciências do Espaço, Faculdade de Ciências da Universidade de Lisboa, Campo Grande, P-1749-016 Lisboa, Portugal*
[21]*School of Physics and Astronomy, University of St Andrews, North Haugh, St Andrews, Fife, KY16 9SS, UK*
[22]*INAF, Osservatorio Astronomico di Trieste, via G.B. Tiepolo 11, I-34143 Trieste, Italy*
[23]*Institute for Fundamental Physics of the Universe, IFPU, Via Beirut 2, I-34151 Grignano, Trieste, Italy*
[24]*European Southern Observatory, Casilla, 19001, Santiago, Chile*

[25]*School of Physics, University of Exeter, Stocker Road, Exeter EX4 4QL, UK*
[26]*European Southern Observatory, Karl-Schwarzschild-Strasse 2, D-85748, Garching b. München, Germany*
[27]*INAF, Osservatorio Astronomico di Cagliari, via della Scienza 5, I-09047, Selargius, Italy*
[28]*INAF, Osservatorio Astronomico di Brera, Via E. Bianchi 46, I-23807 Merate, Italy*
[29]*Astronomy Group, Department of Physics, University of Warwick, Coventry CV4 7AL, UK*
[30]*Astrophysics Research Centre, School of Mathematics and Physics, Queen's University Belfast, BT7 1NN Belfast, UK*

This paper has been typeset from a TEX/LATEX file prepared by the author.